

9644

NATIONAL LIBRARY  
OTTAWA



BIBLIOTHÈQUE NATIONALE  
OTTAWA

NAME OF AUTHOR..... William M. Saunders .....

TITLE OF THESIS..... <sup>to</sup> *Cald, p)* <sup>41</sup> *Ca. Reactions,*  
 ..... *The Statistical Model and*  
 ..... *the Distorted Wave Born Approximation.*

UNIVERSITY..... *of Alberta* .....

DEGREE FOR WHICH THESIS WAS PRESENTED..... *Ph.D.* .....

YEAR THIS DEGREE GRANTED..... *1971* .....

Permission is hereby granted to THE NATIONAL LIBRARY  
 OF CANADA to microfilm this thesis and to lend or sell copies  
 of the film.

The author reserves other publication rights, and  
 neither the thesis nor extensive extracts from it may be  
 printed or otherwise reproduced without the author's  
 written permission.

(Signed)..... *Wm M Saunders* .....

PERMANENT ADDRESS:

..... *502 Michener Park* .....

..... *Edmonton* .....

.....

DATED... *July 15* ..... 19 *71*

THE UNIVERSITY OF ALBERTA

$^{40}\text{Ca}(d,p)^{41}\text{Ca}$  REACTIONS,  
THE STATISTICAL MODEL AND THE  
DISTORTED WAVE BORN APPROXIMATION

by



Wm. M. Saunders

A THESIS

SUBMITTED TO THE FACULTY OF GRADUATE STUDIES  
IN PARTIAL FULFILLMENT OF THE REQUIREMENTS FOR THE DEGREE  
OF DOCTOR OF PHILOSOPHY

DEPARTMENT OF PHYSICS

EDMONTON, ALBERTA

FALL, 1971

UNIVERSITY OF ALBERTA  
FACULTY OF GRADUATE STUDIES

The undersigned certify that they have read,  
and recommend to the Faculty of Graduate Studies for  
acceptance, a thesis entitled  $^{40}\text{Ca}(d,p)^{41}\text{Ca}$  Reactions,  
the Statistical Model and the Distorted Wave Born Approximation,  
submitted by Wm. M. Saunders in partial fulfilment  
of the requirements for the degree of Doctor of Philosophy.

M. Roy  
supervisor  
Barry J. Moulton  
Donald M. Sheppard  
G. H. Williams

James P. Lawrence  
External Examiner

Date June 10, 1971

## ABSTRACT

Yield curves for  $^{40}\text{Ca}(d,\alpha)$  reactions have been measured in the range 4.50 to 5.50 MeV.  $^{40}\text{Ca}(d,p)$  yield curves were obtained from 4.88 to 5.50 MeV; both sets of data were taken in 20 keV energy steps. The yield curves were analyzed for Ericson fluctuations, giving  $\Gamma$ , the average width of a level in the compound nucleus  $^{42}\text{Sc}$  at  $\sim 15$  MeV excitation.  $\Gamma$  was found to be  $\Gamma \leq 23$  keV.

Angular distributions for several  $^{40}\text{Ca}(d,p)$   $^{41}\text{Ca}$  reactions have been measured in the range 4.50 to 5.50 MeV in 2 keV steps. These data were averaged over energy intervals of  $\geq 10 \Gamma$ ,  $\geq 20 \Gamma$  and  $\geq 40 \Gamma$ . The resulting energy averaged angular distributions were then compared with either DWBA or statistical model cross section predictions. It was found that the two smaller averaging intervals are inadequate. Even an averaging interval of  $\geq 40 \Gamma$  is only partially successful in removing energy dependent cross section fluctuations, permitting comparison with theory and the extraction of spectroscopic factors.

## ACKNOWLEDGEMENTS

My supervisor, Gerry Roy, made many important contributions to this thesis, and to my education. The project was his idea, he did the preliminary theoretical investigation, and his beam line is designed to make taking data a pleasure (at least until 3:00 a.m.). This project involved an unusual number of hours on the accelerator--it would have been back-breaking if Gerry hadn't taken regular 12-hour shifts when I was running. He gave me independence when I wanted it, but was always available for advice.

John McDonald, G. C. Neilson, Ken Dawson, J. T. Sample and Doug Sheppard also made valuable contributions. For example, J. T. Sample has taken me aside many times over the past years and explained his well-known "research must be Relevant" theory to me.

Simon Segal spent countless hours in front of a calculator processing the large volume of data. His work was careful and fast, and he saved me months of boring "number crunching". My brother Harry, Gary Sykes and Jim Pasos also helped to crunch.

Jock Elliott keeps the lab in operation. He worked quite a few evenings and weekends to help me get experiments going. I'm sure that we have the only accelerator in the world that produces a high quality beam only in response to salty threats, spoken with a Scots lurr.

Lars, Ron and Paul also worked extra hours to help

me--thanks, fellas.

Dave, Henry, Bob, Norm, Jan, Georges, Titak, Ed, Chung, Sayed, Aadu and Peter helped in various ways, mainly pizzas shared at 3:00 a.m. in the control room and elastic band fights in the grad students' room.

Phyllis McAnally typed this thesis in her spare time for free. She's a mother-in-law with real class.

My wife, Maureen, has spent many lonely evenings and nights since I lost my heart to  $^{40}\text{Ca}$ . Thanks for being patient, Mo.

## TABLE OF CONTENTS

|            |  |    |
|------------|--|----|
| CHAPTER 1  | INTRODUCTION   | 1  |
| CHAPTER 2  | THEORY   | 3  |
| 2.1        | Optical Model  | 3  |
| 2.2        | DWBA   | 7  |
| 2.3        | Compound Nuclear Model   | 13 |
| 2.4        | Interference   | 17 |
| 2.5        | Ericson Fluctuations   | 19 |
| CHAPTER 3  | EXPERIMENTAL   | 22 |
| 3.1        | Scattering Chamber, Detectors and Associated Equipment         | 22 |
| 3.2        | Target Biased  | 25 |
| 3.3        | Targets  | 28 |
| 3.4        | Absolute Cross Sections  | 30 |
| CHAPTER 4  | RESULTS AND DISCUSSION   | 32 |
| 4.1        | Fluctuation Analysis   | 32 |
| 4.2        | Selection of Averaging Intervals                               | 39 |
| 4.3        | Optical Model  | 40 |
| 4.4        | $^{40}\text{Ca}(d,\alpha)^{38}\text{K}$ Reactions              | 44 |
| 4.5        | $^{40}\text{Ca}(d,p)^{41}\text{Ca}$ Compound Nuclear Reactions | 46 |
| 4.6        | $^{40}\text{Ca}(d,p)^{41}\text{Ca}$ Direct Reactions           | 58 |
| 4.7        | Summary and Conclusions  | 67 |
| REFERENCES |  | 69 |

## LIST OF TABLES

|           |  |    |
|-----------|--|----|
| Table 3.1 | Isotopic Composition of Natural Ca                       | 29 |
| Table 4.1 | Starting Values of Optical Model Parameters              | 43 |
| Table 4.2 | Optical Model Parameters Obtained from Experimental Data | 43 |
| Table 4.3 | Deuteron Optical Model Parameters Used for Calculations  | 43 |
| Table 4.4 | Energy Levels of $^{41}\text{Ca}$                        | 47 |
| Table 4.5 | Optical Model Parameters Used in DWBA Calculations       | 58 |
| Table 4.6 | Spectroscopic Factors for States in $^{41}\text{Ca}$     | 65 |



## LIST OF FIGURES

|             |   |    |
|-------------|---|----|
| Figure 2.1  | Shape of Typical Optical Model Potential  | 6  |
| Figure 3.1  | Experimental Arrangement  | 24 |
| Figure 4.1  | Yield Curves for $^{40}\text{Ca}(d,\alpha)$ and $^{40}\text{Ca}(d,p)$   | 33 |
| Figure 4.2  | Autocorrelation Function as a Function of $\Delta$  | 34 |
| Figure 4.3  | Autocorrelation Function as a Function of $\epsilon$  | 34 |
| Figure 4.4  | Level Density for $^{42}\text{Sc}$  | 38 |
| Figure 4.5  | $^{40}\text{Ca}(d,d)$ Elastic Scattering Angular Distribution   | 41 |
| Figure 4.6  | $^{40}\text{Ca}(d,\alpha)^{38}\text{K}$ Angular Distributions   | 45 |
| Figure 4.7  | $^{40}\text{Ca}(d,\alpha)^{38}\text{K}^{0.13}$ Angular Distributions  | 45 |
| Figure 4.8  | $^{40}\text{Ca}(d,\alpha)^{38}\text{K}^{0.45}$ Angular Distributions  | 45 |
| Figure 4.9  | $^{40}\text{Ca}(d,\alpha)^{38}\text{K}^{1.7}$ Angular Distributions   | 45 |
| Figure 4.10 | $^{40}\text{Ca}(d,\alpha)^{38}\text{K}^{2.41}$ Angular Distributions  | 45 |
| Figure 4.11 | $^{40}\text{Ca}(d,p)^{41}\text{Ca}^{3.05}$ Angular Distribution, Averaged Data. Averaging Interval = 250 keV.         | 48 |
| Figure 4.12 | As in Figure 4.11, but Averaging Interval = 500 keV   | 48 |
| Figure 4.13 | As in Figure 4.11, but Averaging Interval = 1000 keV  | 48 |
| Figure 4.14 | $^{40}\text{Ca}(d,p)^{41}\text{Ca}^*$ Angular Distributions for States 7, 8, 10 and 16. Averaging Interval = 1000 keV | 49 |
| Figure 4.15 | Spin Distribution in $^{41}\text{Ca}$   | 52 |
| Figure 4.16 | $^{41}\text{Ca}$ Level Density  | 53 |
| Figure 4.17 | $^{40}\text{Ca}(d,p)^{41}\text{Ca}^{0.0}$ Angular Distributions   | 61 |
| Figure 4.18 | $^{40}\text{Ca}(d,p)^{41}\text{Ca}^{1.95}$ Angular Distributions  | 62 |

---

|             |   |    |
|-------------|---|----|
| Figure 4.19 | $^{40}\text{Ca}(d,p)^{41}\text{Ca}^{2.46}$ Angular Distributions            | 63 |
| Figure 4.20 | $^{40}\text{Ca}(d,p)^{41}\text{Ca}^*$ Yield Curves for States<br>0, 1 and 3 | 64 |

## CHAPTER 1

### INTRODUCTION

In the past decade,  $^{40}\text{Ca} + d$  reactions have been investigated by several groups (e.g. Be65, Mi65). These investigations have produced a great deal of nuclear data; in fact our fairly complete knowledge of most of the exit channels for  $^{40}\text{Ca} + d$  reactions means that a reliable estimate can be made of the compound nuclear contribution to various exit channels using the theory of Hauser and Feshbach (Ha58). (This theory is also known as H-F theory or the statistical model theory.) In other words, we can test H-F theory by comparing its predictions with measured compound nuclear cross sections. Since H-F theory only predicts energy averaged cross sections, angular distributions of protons from  $^{40}\text{Ca}(d,p)$  reactions were obtained in 2keV energy steps from 4.5 MeV to 5.5 MeV bombarding energy. Then the measured cross sections were energy averaged before comparison with H-F predictions.

H-F theory also predicts the average lifetime of compound nuclear states. As explained in Chapter 2, this quantity can be measured by considering the fluctuations in a yield curve; thus we have a further check on the theory.

At the bombarding energies involved in this experiment, two different reaction mechanisms are involved: compound nuclear reactions and direct reactions. These will both be discussed in detail in the theory chapter. As mentioned above, compound nuclear reaction data will be compared to H-F theory; data from direct reactions can be compared to the predictions of the distorted wave Born approximation (DWBA) theory. Lee

et al (Le64) have in fact used the  $^{40}\text{Ca}(d,p)$  reactions as a test of the DWBA. They found that the predictions of the DWBA for the angular distributions were very good, except for poor fits at back angles. It was felt that perhaps a comparison of energy averaged data with DWBA would be more appropriate, at least at low bombarding energies.

In the experiment reported in this thesis, the following measurements were made:

(1)  $^{40}\text{Ca}(d,d)$   $^{40}\text{Ca}$ . Angular distributions of the elastic scattering of deuterons were measured.

Energy averaged distributions were extracted from data taken at 2 KeV intervals from 4.5 MeV to 5.5 MeV. These data were used in the calculation of optical model parameters for use in DWBA and H-F calculations.

(2)  $^{40}\text{Ca}(d,p)$   $^{41}\text{Ca}$ . Energy averaged angular distributions were obtained as in (1), and compared with DWBA and H-F predictions. Also, yield curves were obtained for fluctuation analysis.

(3)  $^{40}\text{Ca}(d,\alpha)$   $^{38}\text{K}$ . Angular distributions were obtained at several bombarding energies. Yield curves were obtained for fluctuation analysis.

## CHAPTER 2

### THEORY

#### 2.1 Optical Model

In both Hauser-Feshbach and DWBA calculations, we need to know the potentials that influence the interacting particles. These potentials are usually obtained from the optical model of the nucleus. In this model we assume that nuclear scattering is analogous to the scattering of light from a translucent sphere.

When a wide beam of light is incident upon a translucent sphere, the following occur:

- (1) part of the beam is reflected;
- (2) part of the beam is absorbed and re-emitted with a phase change (refraction);
- (3) part of the beam is absorbed and re-emitted with a changed frequency;
- (4) part of the beam misses the sphere.

The nucleus is thought of as a sphere of nuclear matter, transmitting, reflecting, refracting and absorbing the incident nuclear waves. Using this model we can understand many phenomena observed in nuclear reactions. For example, interference between the incident and refracted neutron waves explains the complicated broad maxima and minima observed in the total neutron cross section between .1 MeV and a few MeV. The shift of these curves with increasing  $A$  corresponds to diffraction by successively larger spheres.

The optical model of the nucleus is then a complete analog to physical optics. The nucleus can be replaced by a region of fixed refractive index (an attractive potential well) and a given opacity (an imaginary potential well).

The usual version of the optical potential includes a term to account for the spin-orbit interaction. This is necessary to fit polarization data. Also, at the energies used in this investigation, the Pauli principle inhibits collisions, particularly in the dense nuclear interior. Therefore, most absorption takes place near the nuclear surface, and our imaginary potential well must give this effect. The optical potential used has the form

$$U(r) = V_c(r) - V_0 f_{ws}(r, r_0, a) + 4i a_i W \frac{d}{dr} f_{ws}(r, r_0, a) + \left[ \frac{\hbar}{m_p c} \right]^2 V_{so} \frac{d}{dr} f_{ws}(r, r_0, a) \quad \text{I.8} \dots \dots \dots 2.1$$

where (1)  $r$  is the relative separation of the interacting nuclei;

(2)  $V_c(r)$  is the coulomb potential of a sphere of radius  $R = V_0 c A^{1/3}$ , namely

$$V_c(r) = \frac{Z e^2}{r} \left( 3 - \frac{r^2}{R_c^2} \right) \quad r < R_c$$

$$V_c(r) = \frac{Z e^2}{r} \quad r > R_c$$

(3)  $f_{ws}$  is the Wood-Saxon form factor

$$f_{ws} = \frac{1}{1 + \exp[(r - r_0 A^{1/3})/a]}$$

( $r_0$  and  $a$  are radius and diffuseness parameters, respectively)

(4)  $V$  is the strength of the refractive part of the potential.

(5)  $W$  is the strength of the imaginary part of the potential.  $W$  accounts for absorption of particles from the incident beam, i.e. attenuation of the beam. Note that  $W$  is multiplied by the derivative of the Wood-Saxon form factor; this gives the desired peaking of  $W$  at the nuclear surface.

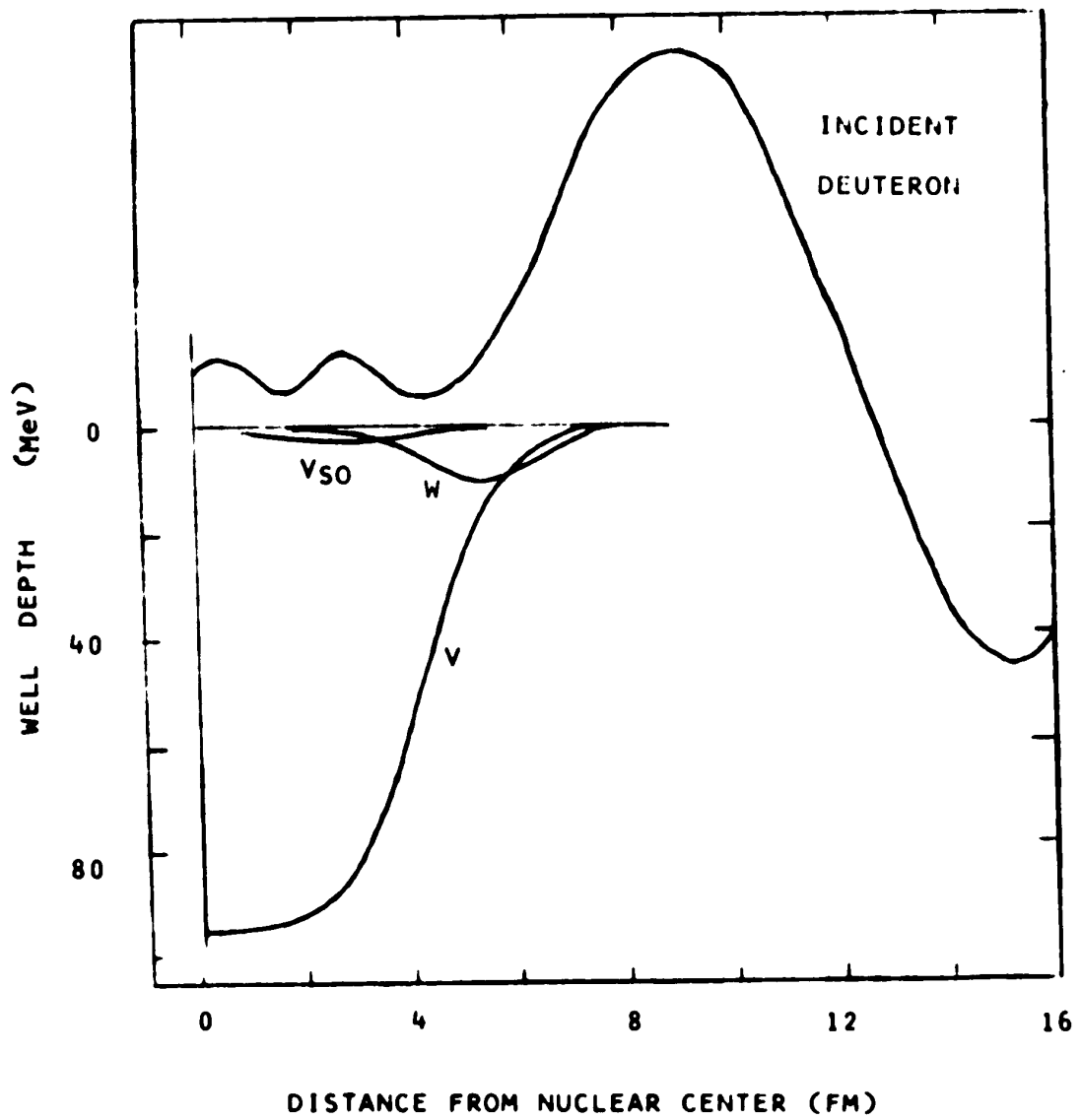
(6)  $V_{so}$  is the strength of a spin-orbit interaction of the Thomas type, which is also peaked at the surface.

(7)  $M_{\pi}$  is the pion mass.

The shapes of  $V$ ,  $W$  and  $V_{so}$ , as well as the real part of the radial wavefunction for  $l=0$  incident deuteron are shown in fig. 2.1. This is taken from Bo69.

Figure 2.1 Typical shapes of real, imaginary and spin-orbit potentials, labelled  $V$ ,  $W$  and  $V_{so}$  respectively. The curve labelled "incident deuteron" shows the real part of the radial wavefunction for an  $l = 0$  deuteron incident on the shown potentials.





## 2.2 DWBA

As mentioned in the introduction, at the bombarding energies used in this experiment two types of reactions are significant--direct reactions and compound nuclear reactions. In this section we will consider direct reactions.

In a direct reaction, the transition from the incident channel (initial state) to the reaction channel (final state) is considered to take place in one step without an intermediate step. The reaction typically takes place in about  $10^{-22}$  sec., the time it would take the incident deuteron to pass the diameter of the target nucleus. A special case of the direct reaction is the stripping reaction. In a stripping reaction, the target nucleus captures part of the incident particle, but not all of it. The remainder of the particle leaves the vicinity of the target without causing further major effects. Thus a direct (d,p) reaction is a stripping reaction.

Consider a stripping reaction  $A(a,b)B$ , where

A is the target nucleus

a is a deuteron

b is a neutron or proton

B is the residual nucleus.

The calculation of the transition amplitude between the initial state (A,a) and the final state (b,B) is performed to the first order only in the interaction potential between the incident particle and the target nucleus. Then, using perturbation theory, we obtain the following expression for

the transition amplitude:

$$T = \langle \phi_f | V' | \psi_i \rangle \dots\dots\dots 2.2$$

where  $\phi_f$  is the asymptotic wavefunction of (b,B)

$\psi_i$  is the initial total wavefunction of the system

$V'$  is the perturbing potential.

(Recall that the cross section is proportional to  $|T|^2$ )

The calculation of T can be greatly simplified by assuming  $\psi_i$  is the product of an incident plane wave and the internal wavefunctions of A and a. This is known as the Born Approximation. Of course, this approximation ignores the distortion of the incident plane wave by the repulsive coulomb force, and the nuclear interaction. If we calculate T using the more appropriate distorted waves, we are making the Distorted Wave Born Approximation or DWBA. These distorted waves are simply the wavefunctions found from solving the Schrodinger equation

$$\nabla^2 \psi(r) + \frac{2u}{\hbar^2} [E - U(r)] \psi(r) = 0 \dots\dots\dots 2.3$$

where u is the reduced mass, U(r) is the optical potential, described in the last section.

Since U(r) is obtained from the analysis of elastic scattering measurements, and since the interaction potential  $V'$  in equation 2.2 is treated as a perturbation, we are implicitly making the assumption that in our reaction elastic scattering predominates, and the other channels make only small contributions.

Now, for a stripping reaction of the type A(d,p)B, the total Hamiltonian of the system can be written as

$$H_t = T_dA + T_{pn} + V_{pn} + V_{pA} + V_{nA}$$

$$= T_nA + T_pB + V_{pn} + V_nA + V_pA \dots\dots\dots 2.4$$

where  $T_dA$  is the operator for the relative kinetic energy of the deuteron-target system

$V_pA$  is the potential energy of the proton-target system, etc.

The Hamiltonian for the final state,  $H_f$ , can be written

$$H_f = T_nA + T_pB + V_nA + \bar{V}_pB \dots\dots\dots 2.5$$

where  $\bar{V}_pB$  is the optical model potential determined from the elastic scattering of protons on B. From equations 2.4 and 2.5 we see

$$V' = H_t - H_f = V_{pn} + V_pA - \bar{V}_pB,$$

where  $V'$  is the perturbing potential in 2.1.

We now make the assumption that

$$V_pA = \bar{V}_pB$$

and we have

$$V' = V_{pn} \dots\dots\dots 2.6$$

(This derivation for  $V'$  follows that of En66).

Substituting 2.6 into 2.2,

$$\begin{aligned} T &= \langle \phi_f | V_{pn} | \psi_i \rangle \\ &= \iint \chi_p^{*(-)}(k_p, r_p) \langle B | V_{pn} | A \rangle \chi_d^{(+)}(k_d, r_d) dr_p dr_d \end{aligned}$$

where  $\chi_d$  and  $\chi_p$  are the incoming deuteron and outgoing proton distorted waves, respectively,  $|A\rangle$  contains the deuteron internal wavefunction and the target nucleus wavefunction,  $\langle B|$  contains the residual nucleus wavefunction. We can simplify the integration by assuming that  $B = A+n$ . Then when we calculate the overlap of the internal wavefunctions of A and B, only the wavefunction of the captured particle remains.

Thus nearly all the physics of the interaction is in the form factor

$$\phi_n V_{pn} \phi_d$$

Here  $\phi_n$  is the wavefunction of the neutron bound to the target nucleus A, and  $\phi_d$  is the internal wavefunction of the deuteron.

A further approximation is now made: the range of  $V_{pn}$  is set to zero, so the product  $V_{pn} \phi_d$  can be replaced by a delta function multiplied by a constant. This implies that the proton appears exactly where the deuteron disappears. This is unsatisfactory because the deuteron is a large, diffuse particle. However, we can simulate the effect of the finite size of the deuteron by multiplying the zero range form factor by a constant correction factor (Bu64), (Pe64). This approach is known as the local energy approximation, and the correction factor is called the finite range correction.

Nuclear forces are thought to be non local--that is the particle interacts with the potential over all space, not only at the center of its wave packet. Thus we should replace  $\psi(r) U(r)$  in the Schrodinger equation (2.3) by  $\int \psi(r') U(r, r') d^3 r'$ . However, to facilitate the calculation we simply multiply the wavefunctions of the local approximation by a constant depending on the real well depth and the range of the nonlocality (Hj65).

Thus, in our direct interaction calculations we have made the following assumptions:

- (1) That the Distorted Wave Born Approximation.

is valid for our experiment;

(2) That  $V = V_{pn}$  (see equation 2.6);

(3) That the internal wavefunction of the residual nucleus is the wavefunction of a neutron bound to the target nucleus. The target nucleus is treated as an inert core.

(4) That the local energy approximation is valid;

(5) Non-local effects can be approximated by multiplying our local wavefunctions by a constant.

All of these assumptions are thought to be reasonable, and in fact are the standard assumptions made for the analysis of stripping reactions.

It is seen in assumption (3) that we are coupling the stripped neutron to an inert  $^{40}\text{Ca}$  core. The probability that for a given state the configuration of the nucleus is that of a single nucleon orbiting about an inert core is the spectroscopic factor for that state. Therefore our calculated cross sections correspond to a spectroscopic factor of 1. We can measure the spectroscopic factor  $S$  of a state by finding the ratio

$$S = \frac{(d\sigma/d\Omega)_{\text{experimental}}}{(d\sigma/d\Omega)_{\text{DWBA}}}$$

The shape of an angular distribution calculated using the DWBA is strongly dependent on  $l$ , the number of units of orbital angular momentum exchanged between the incident particle and the target nucleus. Thus a comparison of experimental and theoretical angular distributions can

give us  $l$ . Furthermore, if the target nucleus has spin and parity  $0^+$ , once  $l$  is determined we know

$$J_f = l \pm 1/2$$

$$\pi_f = (-1)^l$$

where  $J_f$  is the spin of the final state, and  $\pi_f$  is its parity.

### 2.3 Compound Nuclear Model

As mentioned before, we are concerned with two types of reactions: direct reactions and compound nuclear reactions. Direct reactions were discussed in section 2.2; this section deals with compound nuclear reactions. In this type of reaction, the incident particle is completely absorbed by the target nucleus, sharing its energy with some or all of the target nucleons. Eventually, enough of this energy will be acquired by one nucleon or group of nucleons to allow it to escape the system. The time interval between absorption of the incident particle and emission of the outgoing particle is relatively large--typically  $10^{-16}$  seconds when a neutron is absorbed. This means that a fairly long-lived entity has been formed; we call it the compound nucleus.

Reasonable predictions for compound nuclear cross sections can be made by making the following arguments (see Vo69 and references therein).

We consider the reaction



where  $a$  labels the target nucleus, the incident particle, and their state of excitation. ( $a$  is called the entrance channel.)

CN represents the compound nucleus.

$a'$  labels the residual nucleus, the outgoing particle, and their state of excitation.  $a'$  is one of the exit channels.

We assume that



(1) The cross section can be factored into a part representing cross section for formation of the compound nucleus in the entrance channel, and a part representing the probability that the compound nucleus will decay into the appropriate exit channel.

(2) Total angular momentum and parity are conserved.

(3) The optical model can be used to calculate the compound nucleus formation cross sections.

(4) The following reciprocity relation can be used:

$$k_a^2 \sigma_{a\alpha^1} = k_{\alpha^1}^2 \sigma_{\alpha^1 a}$$

where  $k_a$  is the wave number for the relative motion of the pair  $a$

$\sigma_{a\alpha^1}$  is the cross section for the reaction  $a \rightarrow \alpha^1$

$\sigma_{\alpha^1 a}$  is the cross section for the reaction  $\alpha^1 \rightarrow a$

(5) The random phase approximation can be made. Essentially this means that the compound nuclear states are so complicated that the matrix elements connecting a group of them to any other given state are random complex numbers. The matrix elements vary rapidly with energy, both the real and imaginary parts assuming positive and negative values with a mean value of zero. Now, interference between different partial waves is manifested in the theoretical cross section by terms involving the product of different matrix elements. Therefore, if we perform an energy average these inter-

ference terms will cancel because of the statistical fluctuations of the matrix elements about zero. This cancellation of interference gives the characteristic symmetry of the compound nuclear cross section about  $90^\circ$ , as if we were dealing with isolated resonances of definite parity in the compound nucleus.

Because of assumption (5), the model described above is called the statistical model. The model is also called the Hauser-Feshbach model, after the authors who first added conservation of total angular momentum and parity to the theory (Ha52).

With the above assumptions, we obtain the following expressions for compound nuclear cross sections:

$$\bar{\sigma}_{\alpha\alpha'} = \frac{\pi}{k_\alpha^2} \sum_{J, \Pi} \frac{2J+1}{(2I+1)(2i+1)} \left\{ \sum_{s, l} T_l(\alpha) \right\} \left\{ \frac{\sum_{l'} T_{l'}(\alpha')}{\sum_{l''} S_{l''} T_{l''}(\alpha'')} \right\} \dots\dots 2.7$$

where  $\bar{\sigma}_{\alpha\alpha'}$  is the energy averaged total cross section

$I$  and  $i$  are the intrinsic spins of the pair of particles  $\alpha$

$s$  is the channel spin:

$$\tilde{s} = \tilde{I} + \tilde{i}$$

$l$  is the orbital angular momentum of the pair

$J$  is the total angular momentum:

$$\tilde{J} = \tilde{l} + \tilde{s}$$

$\Pi$  is the total parity (the product of  $(-)^l$  with the intrinsic parities of the pair  $\alpha$ )

$T_l(\alpha)$  is the transmission function for the pair

$\alpha$ , given by the optical model phase shift  $\delta_{l\alpha}$ :

$$T_l(\alpha) \equiv 1 - |e^{2i\delta_{\alpha l}}|^2$$

The sum over unprimed quantities is a sum over entrance channels, and the primed quantities are summed over exit channels. The double primed quantities are summed over all possible decay channels.

For differential cross sections

$$\begin{aligned} \frac{d\sigma_{\alpha\alpha'}}{d\Omega} = & \sum_{L=0}^{\infty} \frac{1}{4k_{\alpha}^2} \sum_{J \Pi} \frac{1}{(2I+1)(2i+1)} \left\{ \sum_{s_l} T_l(\alpha) \right\} \\ & \times \sum_{s' l'} \left\{ \frac{T_{l'}(\alpha')}{s'' \sum_{l''} T_{l''}(\alpha'')} \right\} Z(lJlJ; SL) Z(l'Jl'J; S'L) \\ & \times (-)^{S-S'} P_L(\cos \theta) \dots\dots\dots 2.8 \end{aligned}$$

where the Z's are angular momentum coupling coefficients defined by Biedenharn, Blatt & Rose (Bi52).

In both 2.7 and 2.8 we have sums over all possible exit channels in the denominators. In this investigation, decays leaving the residual nuclei in highly excited states were permitted (e.g. 11 MeV for  $^{41}\text{Ca}$ ). Since there is little spectroscopic information available for such exit channels, we are forced to replace the sum over discrete channels by an integration, which requires an estimate of the density of levels as a function of energy. This will be discussed in detail in section 4.5.

Note that for 2.7 or 2.8 to apply, we must energy average our data over a large enough energy interval for the random phase approximation to hold. If this is not done, we cannot expect either symmetry of our compound nuclear cross sections about  $90^\circ$ , or quantitative agreement between measured and predicted cross sections.

## 2.4 Interference

From quantum mechanics we recall that

- (1) The probability of an event in an experiment is given by the absolute value of a complex number  $\phi$  which is called the probability amplitude:

$$P = \text{probability}$$

$$\phi = \text{probability amplitude}$$

$$P = |\phi|^2$$

- (2) When an event can occur in several alternative ways, the probability amplitude for the event is the sum of the probability amplitudes for each way considered separately. There is interference:

$$\phi = \phi_1 + \phi_2$$

let  $\delta$  be the phase difference between  $\phi_1$  and  $\phi_2$

$$P = |\phi_1 + \phi_2|^2$$

$$\approx |\phi_1|^2 + |\phi_2|^2 + 2|\phi_1||\phi_2| \cos \delta$$

$$P = P_1 + P_2 + 2 P_1 P_2 \cos \delta \dots\dots\dots 2.9$$

Thus the overall probability is the probability that the event occurs by mechanism 1 plus the probability that the event occurs by mechanism 2, plus a term indicating interference between the two mechanisms. (This treatment is from reference Fe65).

In this experiment, we are measuring cross sections of states that can be formed either by direct or compound nuclear reactions. In this context equation 2.9 can be written:

$$\sigma_T = \sigma_{CN} + \sigma_D + 2 \sigma_{CN} \sigma_D \cos \delta$$

where  $\sigma_T$  is the total cross section  
 $\sigma_{CN}$  is the compound nuclear cross section  
 $\sigma_D$  is the direct cross section.

In the most general case, then, part of the total cross section comes from the interference between the direct and compound nuclear mechanisms. However, if we obtain energy averaged cross sections so that the random phase approximation is valid, the phase differences between the direct and CN amplitudes will be random numbers, fluctuating rapidly with energy about a mean of zero. Thus, the interference terms cancel and we are left with

$$\bar{\sigma}_T = \bar{\sigma}_{CN} + \bar{\sigma}_D$$

where  $\bar{\sigma}$  is an energy averaged cross section.

It should be noted that it is still debatable as to whether or not interference between direct and CN amplitudes has ever been observed. Many investigators simply assume that direct and compound nuclear reactions are incoherent, i.e. that interference is negligible. This assumption probably introduces a much smaller error than the errors inherent in DWBA and Hauser-Feshbach calculations.

## 2.5 Ericson Fluctuations.

As explained in section 2.3, if we measure a cross-section as a function of energy, we will observe fluctuations above and below the mean cross-section unless the random phase approximation holds. Such a yield curve is made up of overlapping compound nuclear resonances which may interfere constructively or destructively, giving rise to the fluctuations.

Ericson noted that these fluctuations could be exploited to give information about compound nuclear properties (ER63). If the overlapping resonances have an average width  $\Gamma$ , a particular resonance will influence the yield curve over an energy range of approximately  $\Gamma$ . Now compare the cross-section at two energies,  $E$  and  $E + \epsilon$ :

- (1) if  $\epsilon \ll \Gamma$ , then at both energies the same resonances contribute to the cross-section, and the two cross-sections will be quite similar;
- (2) if  $\epsilon \gg \Gamma$ , different resonances predominate at the two energies, and the cross-sections will be uncorrelated.

Thus, by measuring the correlation of the cross-sections as a function of  $\epsilon$ , we can estimate  $\Gamma$ . The correlation is measured using the autocorrelation function:

$$C(\epsilon) = \frac{\langle [\sigma(E) - \bar{\sigma}] [\sigma(E + \epsilon) - \bar{\sigma}] \rangle}{(\bar{\sigma})^2}$$

where  $\langle \dots \rangle$  is an energy average

$E$  is the energy

$\bar{\sigma}$  is the average cross section.

Once  $\Gamma$  has been measured, we can obtain the average compound nuclear lifetime using the uncertainty principle:

$$\Gamma \tau \approx \hbar$$

where  $\tau$  is the average CN lifetime.

$\tau$  can be predicted by a Hauser-Feshbach calculation and compared to the measured value.

Often a fluctuation analysis is done on a state that has a significant direct reaction cross section. Thus, the fluctuations due to CN reactions are superimposed on a direct reaction cross-section. Ericson derived a form of the autocorrelation function for such a situation:

$$C(\epsilon) = \frac{1}{N} (1 - a_D^2) \frac{\Gamma^2}{\epsilon^2 + \Gamma^2}$$

where  $N$  is the fluctuation damping coefficient (see below)

$a_D$  is the ratio of direct to total cross-section.

Since we are using an unpolarized beam, contributions from different spin projections are incoherent. If there are  $N$  equivalent incoherent contributions, the fluctuations in the yield curve will be reduced by  $1/\sqrt{N}$ . Near  $90^\circ$ , an approximate value for  $N$  is

$$N = \frac{1}{2} [(2I+1)(2i+1)(2I^1+1)(2i^1+1)]$$

where  $i$  is the spin of the incident particle

$I$  is the spin of the target nucleus

$i^1$  is the spin of the outgoing particle

$I^1$  is the spin of the residual nucleus.

Unfortunately, the finite range of data errors (see below) made it impossible to extract meaningful values for  $\alpha_D$  from this experiment. To obtain  $\alpha_D$  the yield curves could have been taken over a much larger energy range; time limitations made this unfeasible.

The main error in a fluctuation analysis comes from the finite energy span of experimental yield curves. In other words, if more CN resonances enter into our experimental yield curve (i.e. if we extend the measurement over a larger energy range) we can determine  $\Gamma$  more accurately. Expressions estimating the errors introduced by the finite range of data have been derived (Pa65).



## CHAPTER 3

### EXPERIMENTAL

#### 3.1 Scattering chamber, detectors and associated equipment.

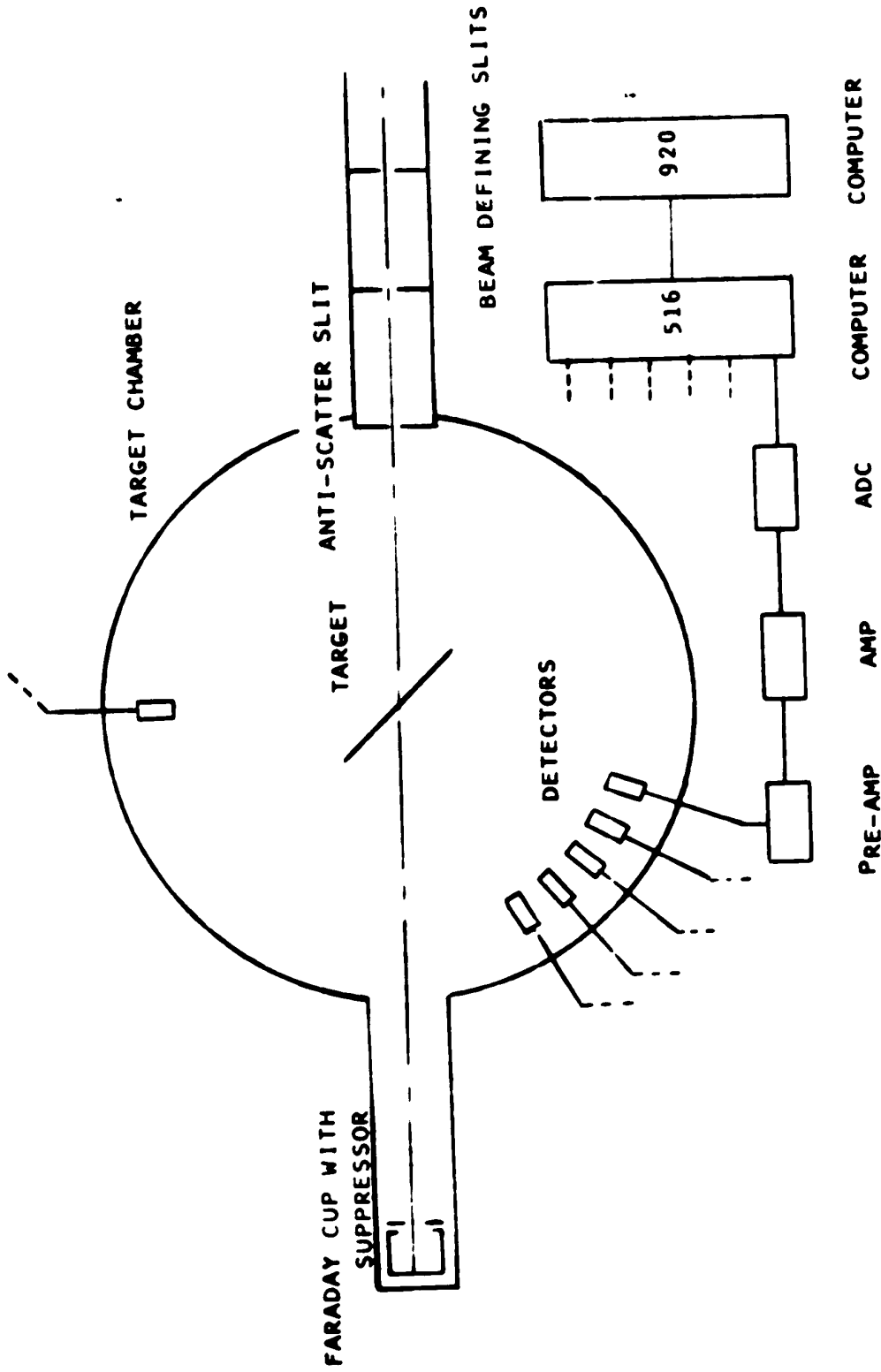
The incident deuteron beam for this experiment was produced by the University of Alberta CN type Van de Graaff accelerator. The measurements were taken in a 16" scattering chamber designed by Dr. G. Roy. Five silicon surface barrier detectors were used, simultaneously collecting data at different angles. Circular collimators were placed in front of each detector. They subtended a solid angle of about  $2 \times 10^{-4}$  steradians. The relative solid angles of the collimators were measured by placing each detector at a given angle in turn and observing protons elastically scattered from gold. To decrease noise and improve resolution in the detectors, they were cooled with an ethanol-dry ice mixture. For the angular distributions, four movable detectors were mounted  $10^\circ$  apart at a distance of 8" from the center of the chamber. A fifth detector held stationary at  $90^\circ$  was used as a monitor. For the yield curves, five stationary detectors were mounted 8" from the center. The voltage pulses from each detector were processed by a pre-amplifier, an amplifier and an analog to digital converter (ADC) in turn. That is, there were five independent systems, consisting of detector--pre-amp--amp--ADC. Each ADC was connected to a clock for dead time measurements. The output of the five ADC's was stored in the data acquisition computer (a Honeywell 516). At the end of a run, the data were transferred to the data analysis computer (an SDS 920) for writing the data on magnetic tape, summing

peaks, plotting spectra etc. (See fig. 3.1). As soon as the data were transferred to the 920, the 516 was free and a new run was begun. This saved many hours of machine time, since data collection, storage and analysis could be carried out at the same time rather than sequentially.

The beam was collimated by two adjustable beam defining slits and an anti-scatter slit, (Ro69a). The beam defining slits were adjusted to minimize background counts. After passing through the target and out of the scattering chamber, the beam was collected in a Faraday cup. A secondary electron suppressor biased to - 1000V was mounted slightly in front of the Faraday cup.

**Figure 3.1**

**Schematic of Experimental Arrangement.**



### 3.2 Target biaser.

As mentioned in the theory section of this thesis, experimental compound nuclear cross sections must be energy averaged before comparison with Hauser-Feshbach predictions. In other words, we must obtain cross sections at a number of bombarding energies in a large enough energy range that the random phase approximation holds, and then average the cross sections. There are several ways in which data can be obtained for a range of bombarding energies:

- (1) If a very thick target is used, the beam energy is degraded over an appreciable energy range. This method is used very frequently in gamma ray spectroscopy--e.g. see Pi70. However, outgoing particles are also degraded over a large energy range if they can get out of the target at all, so this method is not acceptable for high resolution charged particle work.
- (2) The terminal voltage of the Van de Graaff can be changed. In this method we measure cross sections at one energy, slightly change the bombarding energy, measure the cross sections again, and so on. After the run the cross sections are averaged manually. This is obviously very tedious and consumes large amounts of machine time.
- (3) A voltage can be applied to the target to slow down the bombarding particles. If the outgoing particles have the same charge as the incoming particles, they will arrive at the detectors with

almost exactly the same energy for all values of the bias voltage applied to the target. For example, by applying a bias voltage continuously varying between 0 and 50 kv during a run, we can simulate the effect of a thick target, but retain good resolution by actually using a thin target.

In this investigation, a combination of (2) and (3) was used for the (d,p) work. During a run, the target bias was stepped between 0 and + 50 kv in two kv steps. After an angular distribution was completed, another was taken 50 keV lower in bombarding energy. Essentially, we have taken  $^{40}\text{Ca}(d,p)$  angular distributions every 2 keV from 4.50 to 5.50 MeV bombarding energy. We have automatically averaged cross sections over 50 keV intervals, and manually averaged the 50 keV averaged cross sections over larger intervals. Since deuterons are singly charged and alpha particles are doubly charged, this technique cannot be used for high resolution (d, $\alpha$ ) work.

The target biasing system consisted of a 0 to 60 kV dc power supply connected to the target. An automatic controller for the system was designed by Dr. G. Roy and Mr. L. Holm (Ro71). In the automatic mode, the system functioned in the following way:

The Van de Graaff terminal voltage was set for a particular deuteron bombarding energy, and the bias on the target was set to zero. The run was begun, and the amount of beam passing through the target was monitored by measuring the amount of charge collected at the Faraday cup. After a

specific amount of beam had passed through the target, the control system temporarily stopped the run, incremented the target bias by + 2 kV, and restarted the run. The bombarding energy was then 2 keV lower than previously. When + 50 kV bias was reached by this process, two runs at that voltage were taken; then the bias voltage was automatically decreased by 2 kV per step. The run was continued until 0 kV bias was reached again; data were taken at 0 kV and then the run was terminated. Thus, we made two measurements at every target bias voltage between 0 and + 50 kV inclusive. The cross sections measured from the resulting spectra were therefore already averaged over a 50 keV energy range.

### 3.3 Targets

Targets were made by evaporating natural calcium onto backings of thin carbon on formvar. (See table 3.1 for the isotopic abundances of natural calcium.) The carbon layer was necessary to dissipate the heat generated by the beam; it was kept very thin in order to minimize its effect on energy resolution. The formvar layer was necessary for mechanical strength. The calcium was evaporated onto the formvar rather than the carbon, since it has been found that the calcium apparently reacts with the carbon and weakens the target (Bo69).

About 30  $\mu\text{g}/\text{cm}^2$  of calcium was deposited on the backings. This gives an energy loss of  $\leq 5$  keV in the target.



Table 3.1

| <u>Calcium Isotope</u> | <u>% abundance</u> |
|------------------------|--------------------|
| 40                     | 96.97              |
| 42                     | 0.64               |
| 43                     | 0.145              |
| 44                     | 2.06               |
| 46                     | 0.0033             |
| 48                     | 0.18               |

### 3.4 Absolute cross sections.

In order to measure absolute cross sections in an experiment, we must obtain a factor that will convert relative cross sections (e.g. the number of events observed in a particular reaction, suitably normalized) to absolute cross sections (e.g. the cross section for a particular reaction in millibarns per steradian). This was done in slightly different ways for the  $^{40}\text{Ca}(d,\alpha)$  experiment and the  $^{40}\text{Ca}(d,p)$  experiment.

(a)  $^{40}\text{Ca}(d,\alpha)$ . The elastic scattering of 2.0 MeV protons from  $^{40}\text{Ca}$  was measured at 30, 40, 50 and 60 degrees. This reaction proceeds almost exclusively by the Rutherford scattering mechanism. Since the Rutherford differential cross section is a function of the bombarding particle's charge and energy, the charge of the target nucleus, and the angle of observation only, it can be easily calculated. Then the number of counts observed at each angle can be corrected for electronic dead time and collimator size, and the ratio  $\frac{\text{millibarns/steradian}}{\text{normalized count}}$  for a given amount of beam passing through the target can be determined. This factor can then be used to convert the number of counts to absolute cross sections for other reactions at other energies, providing the same normalizations are made for collimator sizes, dead times and the amount of beam. As a check, during the (d, $\alpha$ ) angular distributions occasional runs were made at 5.00 MeV, and the  $^{40}\text{Ca}(d,d)$  elastic peak was summed.

The absolute (d,d) cross section was then compared to the values reported by Leighton (Le68). These check runs were always consistent with Leighton's results, within experimental errors. The (d, $\alpha$ ) data were obtained in a series of five runs, all using the same target. The  $^{40}\text{Ca}(p,p)$  measurement was made after each of these runs. No evidence of target deterioration was found.

(b)  $^{40}\text{Ca}(d,p)$ . These data were obtained in eight runs, using four different targets. The absolute cross sections were determined in much the same way as in (a). The only difference was that for check runs, data was taken at 5.00 MeV with no target bias, and the  $^{40}\text{Ca}(d,p)$   $^{41}\text{Ca}^{0.0}$  peak was summed, and compared to the work of Leighton (Le68). This peak was not observed in the d, $\alpha$  work, since detectors with a thin depletion zone were used for that work: i.e. the high energy protons were not stopped in the active region of the detectors. However, this peak is actually preferable for a consistency check since it is in a region of no background and has a fairly high cross section at forward angles.

## CHAPTER 4

### RESULTS AND DISCUSSION

#### 4.1 Fluctuation Analysis.

Using the experimental configuration described in Section 3.1, yield curves were taken for the  $^{40}\text{Ca}(d,p)$  and  $^{40}\text{Ca}(d,\alpha)$  reactions. The  $(d,\alpha)$  yield curve was measured from 4.50 to 5.50 MeV, while the  $(d,p)$  measurements were in the range 4.88 to 5.50 MeV. (The discrepancy in the two ranges was unplanned. It occurred when the last  $^{40}\text{Ca}$  target broke near the end of the time allotted for the measurement.) Both yield curves were taken in 20 keV steps. Measurements were made at 70, 100, 120, 150 and 170°. Representative results are shown in figure 4.1.

Using these data, the autocorrelation function was calculated for each excitation curve. Recall from Chapter 2, part (5), that the autocorrelation function  $C(\epsilon)$  is given by

$$C(\epsilon) = \frac{\langle [\sigma(E) - \bar{\sigma}][\sigma(E+\epsilon) - \bar{\sigma}] \rangle}{(\bar{\sigma})^2}$$

where  $\langle \dots \rangle$  is an energy average

$E$  is the energy

$\bar{\sigma}$  is the average cross section.

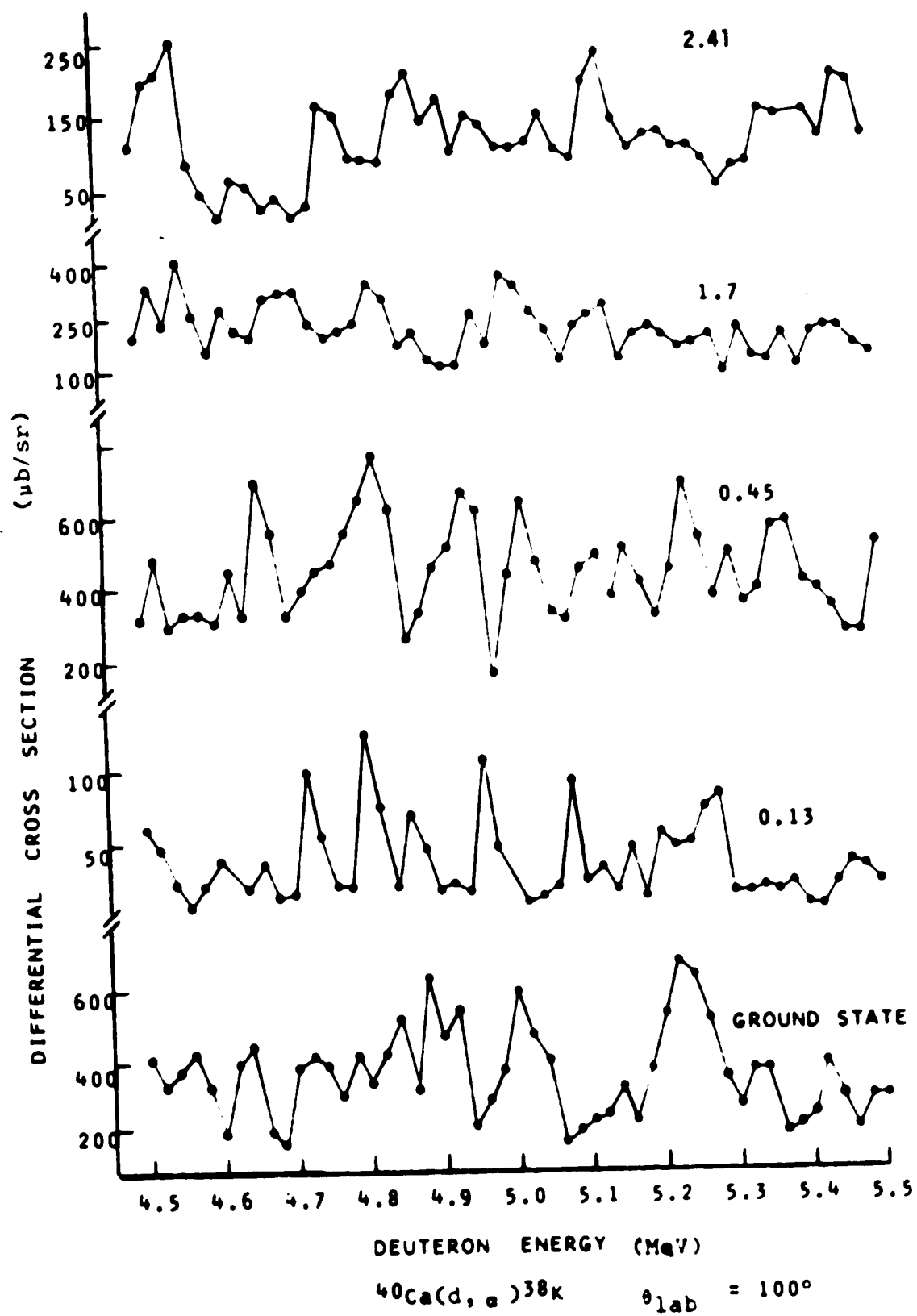
Generally, the Ericson fluctuations will be superimposed upon coarser structure in the yield curve. Thus,  $\bar{\sigma}$  is a function of energy. In this study,  $\bar{\sigma}$  was calculated using the "sliding average" (SA) method of Pappalardo (Pa64). In the SA method, the experimental yield curve is broken up into energy intervals  $\Delta$ .  $\bar{\sigma}$  is calculated for each interval and the entire set of values of  $\bar{\sigma}$  as a function of energy

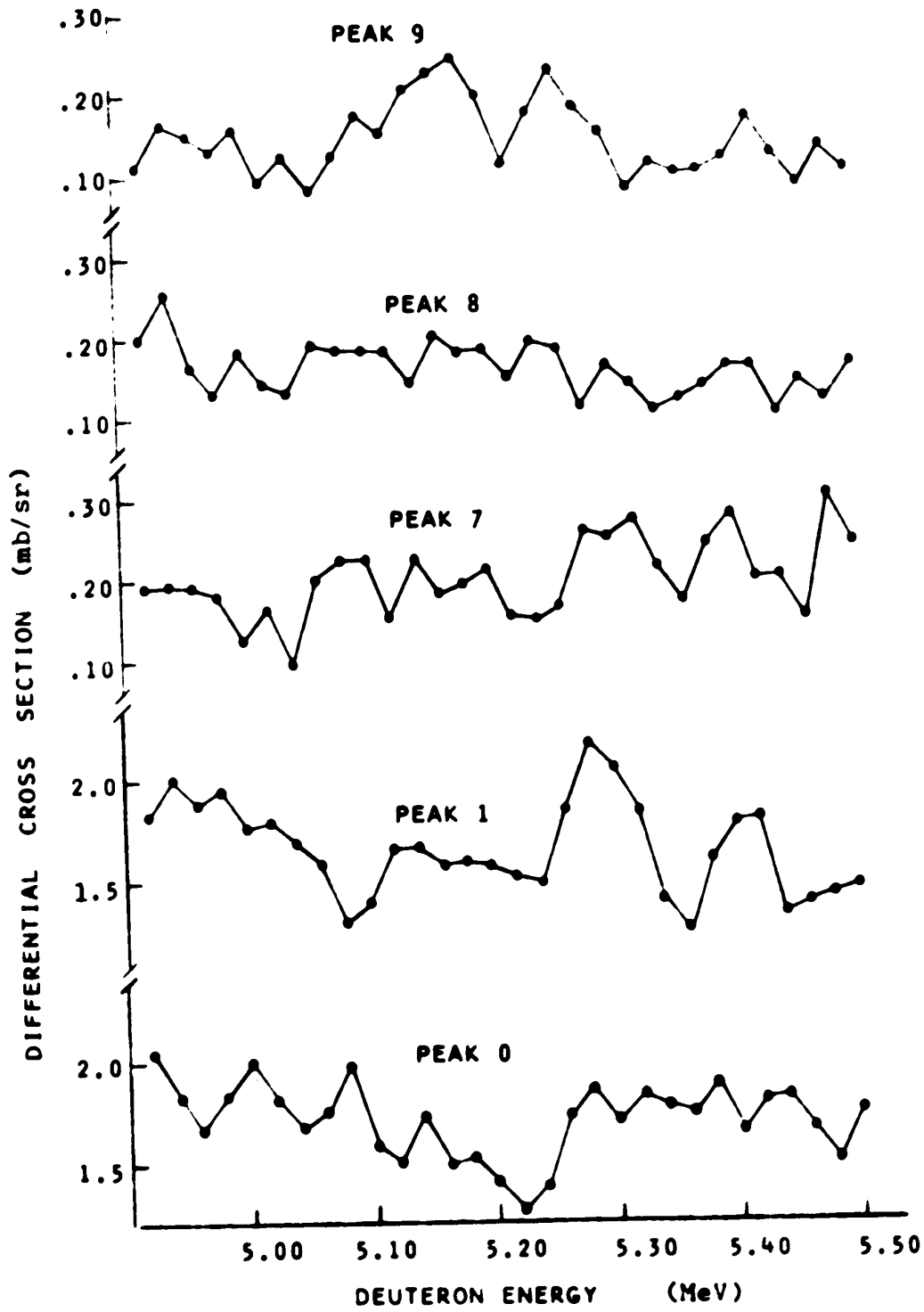
Figure 4.1

A)  $^{40}\text{Ca}(d,\alpha)^{38}\text{K}$  yield curves. Lab angle =  $100^\circ$ .

B)  $^{40}\text{Ca}(d,p)^{41}\text{Ca}$  yield curves. Lab angle =  $100^\circ$ .

In both cases, the statistical error is less than the size of the data points.





$^{40}\text{Ca}(d,p)^{41}\text{Ca}$ ,  $\theta_{\text{lab}} = 100^\circ$

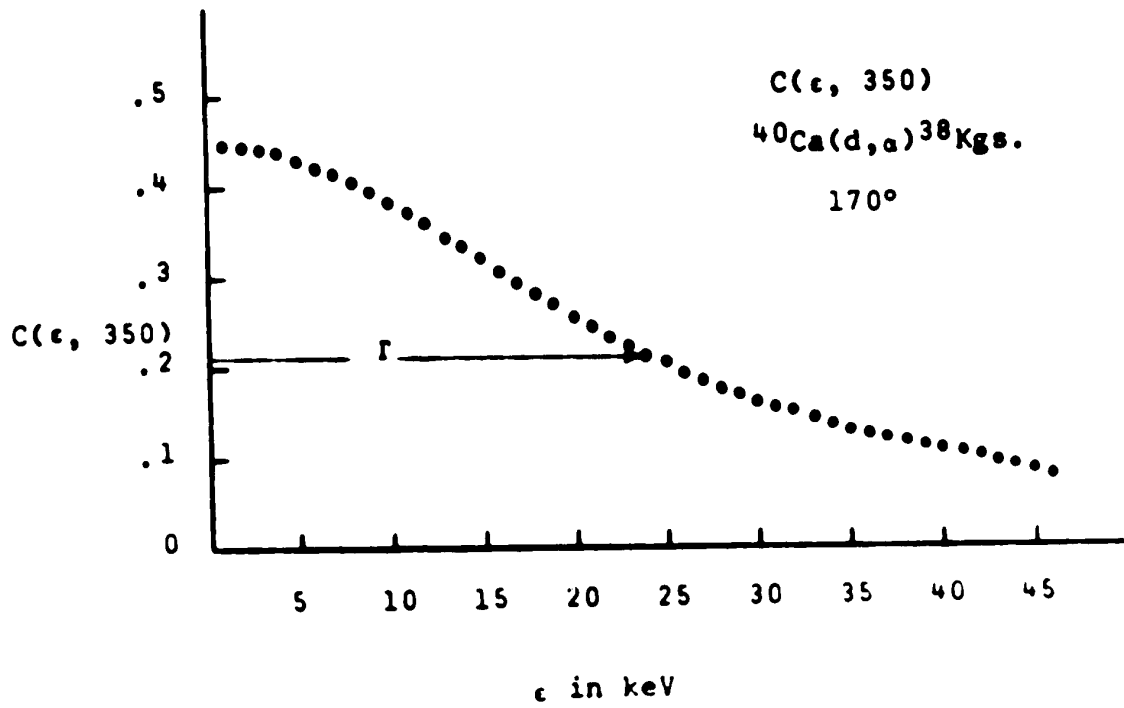
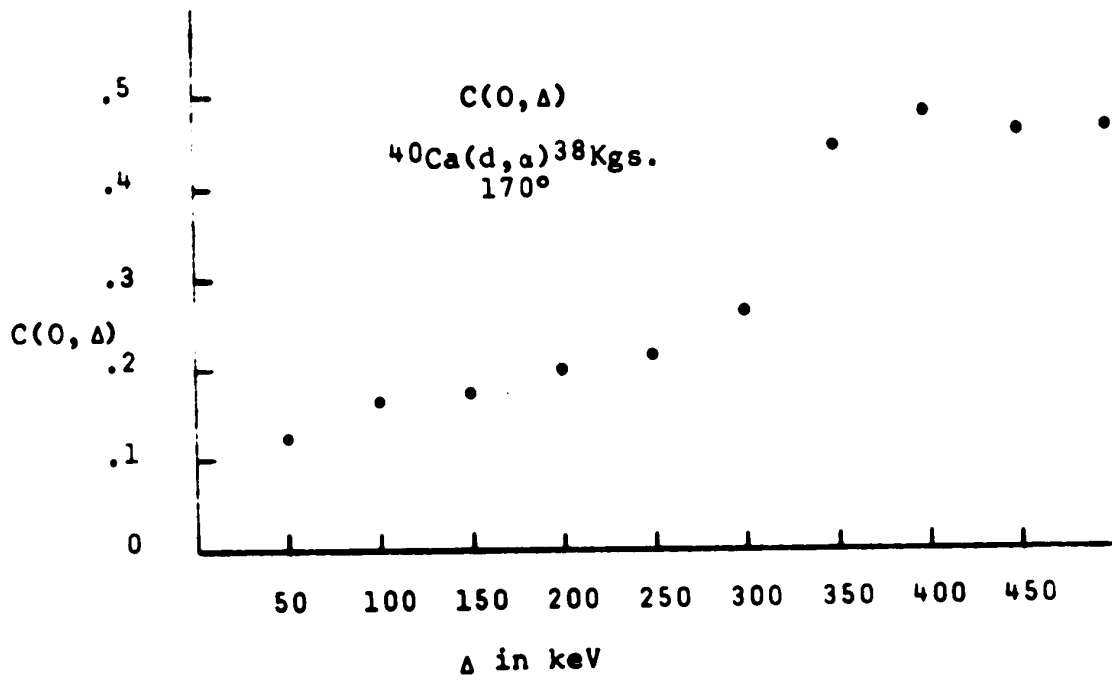
**Figure 4.2**

Autocorrelation function with  $\epsilon = 0$  as a function of  $\Delta$ , the averaging interval. The calculation is for the  $^{38}\text{K}$  ground state yield curve at  $170^\circ$ .

**Figure 4.3**

Autocorrelation function with  $\Delta = 350$  keV as a function of  $\epsilon$ . The calculation is for the same data as in fig. 4.2.





is obtained by interpolating between these values.  $\bar{\sigma}$  is a function of  $\Delta$ , thus the autocorrelation function is also a function of  $\Delta$ . Figure 4.2 shows the behavior of  $C(\epsilon=0, \Delta)$  with change in  $\Delta$ . A value of  $\Delta$  is selected on the "plateau" where  $C(\epsilon=0, \Delta)$  does not change with  $\Delta$ .  $C(\epsilon)$  is then calculated varying  $\epsilon$ . Typical results are shown in figure 4.3. The width at half maximum of this curve is  $\Gamma$ , the average width of a compound nuclear level.

$\Gamma$  was calculated by this method for each observed state in the residual nuclei, at each angle. After taking an average of the  $\Gamma$ 's obtained, the average width of a level in  ${}^{42}\text{Sc}$  at  $\approx 15$  MeV excitation was found to be  $18.5$  keV. (The error quoted is the finite range of data error - see Chapter 2, section 6).

It is somewhat disturbing to note that the value for  $\Gamma$  is essentially equal to  $\Delta E$ , our energy increment in the yield curve. Although some yield curves have been analyzed with  $\frac{\Delta E}{\Gamma} > 1$  (e.g. Bi70), it seems preferable to have  $\frac{\Delta E}{\Gamma} < 1$ . It has been suggested that measurements with  $\frac{\Delta E}{\Gamma} > 1$  tend to erroneously give values of  $\Gamma \approx \Delta E$ , (Da69). Because of this, it is felt that the quoted value for  $\Gamma$  must be viewed with some suspicion. However, an upper limit for  $\Gamma$  has definitely been established:  $\Gamma \leq 23$  keV. This information is very useful in determining the energy range over which measured cross sections must be averaged before comparison with the statistical model. This will be discussed further in section 2 of this chapter.

A theoretical value for  $\Gamma$  can be obtained by a

Hauser-Feshbach calculation. This involves evaluating the following integral:

$$\Gamma \propto \int \frac{\sigma_{\nu}(\epsilon, E_x - \epsilon) W_{\nu}(E_x - \epsilon) d\epsilon}{W_C(E_x)} \dots\dots\dots 4.1$$

where

$\nu$  labels the type of outgoing particle

$E_x$  = excitation of compound nucleus

$\epsilon$  = energy of outgoing particle

$W_C(E_x)$  = level density of compound nucleus at  $E_x$  MeV excitation

$W_{\nu}(E_x - \epsilon)$  = level density of residual nucleus at  $E_x - \epsilon$  MeV excitation

$\sigma_{\nu}(\epsilon, E_x - \epsilon)$  = cross section of inverse reaction, i.e. capture of the appropriate particle incident at  $\epsilon$  MeV on the target excited to  $E_x - \epsilon$  MeV.

$\Gamma$  was calculated using the program HAUSER†. All of the quantities in 4.1 are well known except  $W_C$ , the level density of the compound nucleus  $^{42}\text{Sc}$ . Level densities are passed to HAUSER in the following manner. Let  $N(E_x)$  be the number of levels below an excitation energy  $E_x$ . Then a plot of  $\log N(E_x)$  vs.  $\sqrt{E_x}$  is close to a straight line, the deviations becoming less and less as  $E_x$  increases. The slope and intercept of the line determine the level density; these quantities are given to HAUSER.

Figure 4.4 is a plot of  $\log N(E_x)$  vs.  $\sqrt{E_x}$  for  $^{42}\text{Sc}$ . Fifteen levels are known in this nucleus to an excitation of 3.36 MeV. Clearly, this is not enough to

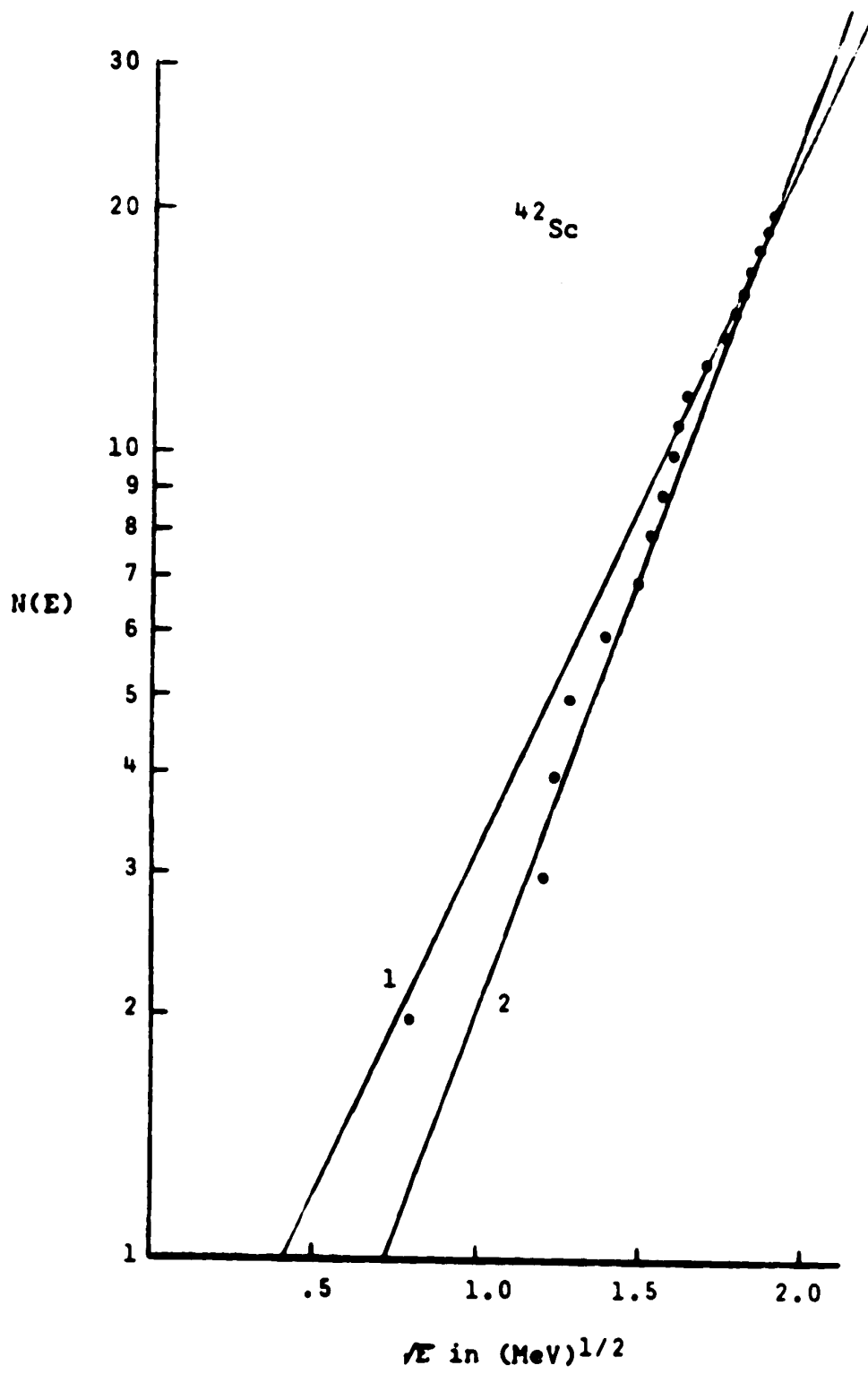
†Obtained from W. R. Smith of the Oak Ridge National Laboratory and modified by N. E. Davison of this laboratory.

define a unique line. Limiting cases can be estimated however, and lines 1 and 2 in figure 4.13 correspond to  $\Gamma$ 's of 15 and 40 keV respectively. To summarize, we find theoretically  $15 < \Gamma < 40$ ; experimentally  $\Gamma < 23$ .

It should be noted at this time that  $W_c$  does not enter the Hauser-Feshbach calculation of the cross sections for formation of particular states in residual nuclei. Therefore our inadequate knowledge of this parameter only affects our predictions for  $\Gamma$ ; absolute cross sections can be predicted much more accurately.

Figure 4.4

Level density for  $^{42}\text{Sc}$  (the compound nucleus in this study). The two curves (1 and 2) through the data are of the form  $\log N = a + b \sqrt{E}$ . Both give acceptable fits to the data; this illustrates the difficulty in determining the level density of  $^{42}\text{Sc}$  from the existing data.



#### 4.2 Selection of Averaging Intervals.

Recall from Chapter 2, part (3) that, for comparison of measured compound nuclear cross sections with Hauser-Feshbach predictions, the data must be energy averaged over a large enough energy interval for the random phase approximation to hold. This will also eliminate any direct-compound nuclear interference (Chapter 2, part 4). It is often assumed that an interval of  $20 \Gamma$  is sufficient for this (e.g. St70). In this study, intervals of 250 keV ( $\approx 10\Gamma$ ), 500 keV ( $\approx 20\Gamma$ ) and 1000 keV ( $\approx 40\Gamma$ ) were used for purposes of comparison.

### 4.3 Optical Model.

Optical model parameters for the  $^{40}\text{Ca}+d$  system were obtained from the measured  $^{40}\text{Ca}(d,d)^{40}\text{Ca}$  elastic scattering using the computer code SNOOPY 2\*. This program will search over up to six of the optical model parameters to give a best fit to the experimental data.

From the nature of the optical model, we expect the parameters to vary slowly and smoothly with bombarding energy. It has been found that the optical model parameters that give the most satisfactory results for  $^{48}\text{Ca}(d,p)^{49}\text{Ca}$  DWBA calculations are energy averaged parameters. (Bo69). That is, the elastic scattering is measured at several energies, several sets of optical model parameters are extracted, and these parameters are averaged. These average parameters are then used for DWBA calculations at all energies. In Bo69, this gave superior results to DWBA calculations using parameters obtained from elastic scattering measurements only at the energy in question. This suggests that the measurement of elastic scattering cross sections at one energy is insufficient to obtain good optical model parameters, even when they are to be used for DWBA calculations for reactions occurring at that same energy. For this reason, the parameters were obtained from elastic scattering data that had been averaged over 1 MeV. (The data were taken from 4.50 to 5.50 MeV in 2 keV steps). These average cross sections are presented in figure 4.5.

SNOOPY varies the optical model parameters to

\*Obtained from W. Haerberli, University of Wisconsin, Madison, Wisconsin.

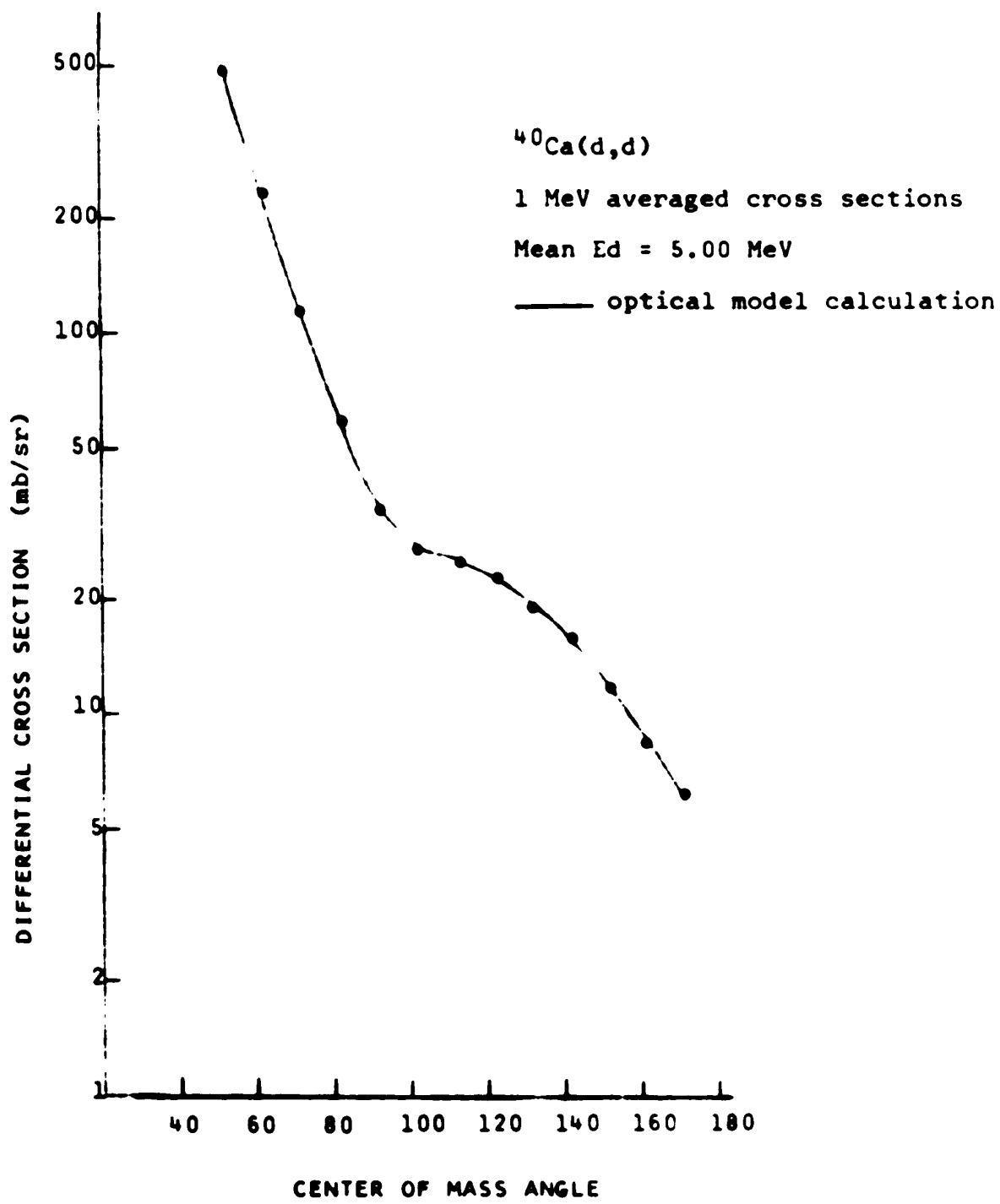


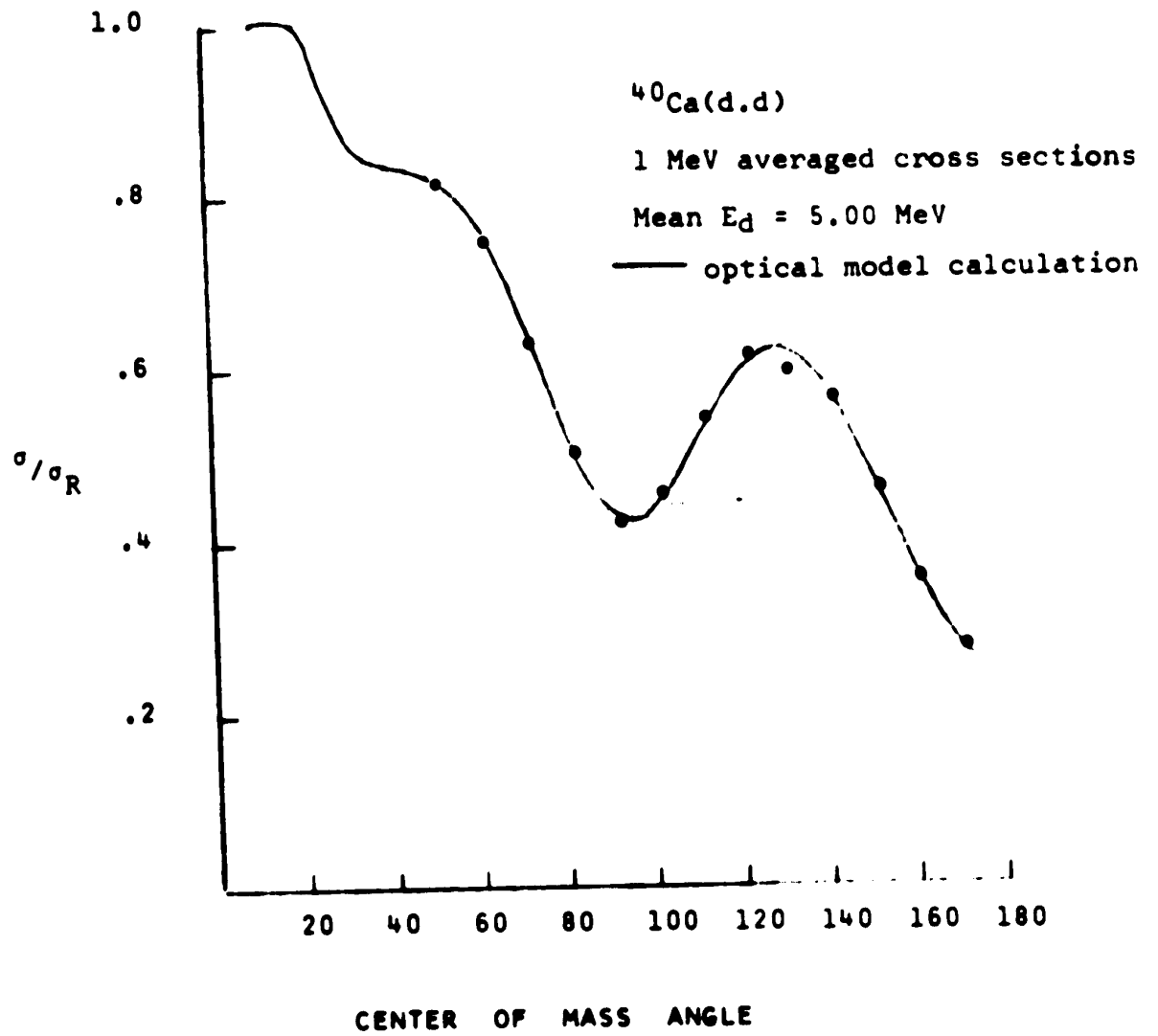
Figure 4.5

$^{40}\text{Ca}(d,d)$  elastic scattering angular distribution.

Data is averaged over 1 MeV with the mean bombarding energy = 5.00 MeV. The theoretical curve is generated from the optical model. The parameters used in the calculation are given in table 4.2. Statistical errors are less than the size of the points.

- A) differential cross section vs. angle
- B) ratio differential cross section/differential Rutherford cross section vs. angle.





give the best fit of optical model theoretical cross sections to the experimental data. The "goodness of fit" is measured by  $\chi^2$ :

$$\chi^2 = \sum_{i=1}^m \left[ \frac{\sigma_{\text{calc}}(\phi_i) - \sigma_{\text{exp}}(\phi_i)}{\Delta\sigma_{\text{exp}}(\phi_i)} \right]^2$$

where the sum is over all experimental angles

$\sigma_{\text{calc}}(\phi_i)$  is the optical model differential cross section at angle  $\phi_i$ .

$\sigma_{\text{exp}}(\phi_i)$  is the corresponding measured cross section.

$\Delta\sigma_{\text{exp}}(\phi_i)$  is the error in the measured cross section.

In this study,  $\sigma_{\text{exp}}(\phi_i)$  is the differential elastic cross section, minus the Hauser-Feshbach contribution.

SNOOPY generates sets of optical model parameters by minimizing  $\chi^2$  while searching over the optical model parameters. Since the search is carried out in a 9-dimensional parameter space, it is very easy for the program to become "trapped" in local minima. To avoid this, the sequence in which parameters are searched, and the limits of the search must be chosen very carefully. In this study, the method suggested by Bogaards (Bo69) was used:

- (1)  $V_{\text{so}}$ ,  $r_{\text{so}}$  and  $a_{\text{so}}$  were fixed at reasonable values;
- (2)  $V$  and  $a_i$  were stepped through a reasonable range of values;
- (3)  $r_o$ ,  $a$ ,  $w$  and  $r_i$  were searched simultaneously for each value of  $V$  and  $a_i$ . The starting values for the searches were the parameters given by Schwandt and Haerberli (Sc69), and are summarized in Table 4.1.

Table 4.1Initial values of optical model parameters for search

| $r_o$   | $a$     | $w$     | $r_i$   | $V_{so}$ | $r_{so}$ | $a_{so}$ |
|---------|---------|---------|---------|----------|----------|----------|
| 1.05 fm | 0.85 fm | 8.5 MeV | 1.66 fm | 9 MeV    | 0.9 fm   | 0.6 fm   |

$V$  was stepped from 80 MeV to 125 MeV in 5 MeV increments, while  $a_i$  varied from 0.30 to 0.80 fm in 0.05 fm increments. (Schwandt and Haeberli found 112 MeV and 0.52 fm for  $V$  and  $a_i$ .)

Table 4.2 gives the results of this procedure:

Table 4.2Optical model parameters generated from 1 MeV averaged elastic scattering data.

| $V$    | $r_o$   | $a$     | $w$      | $r_i$   | $a_i$   |
|--------|---------|---------|----------|---------|---------|
| 95 MeV | 1.21 fm | 0.71 fm | 6.70 MeV | 1.47 fm | 0.70 fm |

Figure 4.5 shows the cross sections calculated from the optical model using these parameters and the 1 MeV averaged elastic scattering cross sections. In this study, calculations were done with two sets of optical model parameters: the above set, and those of Schwandt and Haeberli. These are compared in table 4.3.

Table 4.3Optical model parameters used for calculations.

Set I--generated from 1 MeV averaged elastic scattering data.

Set II--from Schwandt and Haeberli (Sc69).

|        | $V$<br>(MeV) | $r_o$<br>(fm) | $a$<br>(fm) | $w$<br>(MeV) | $r_i$<br>(fm) | $a_i$<br>(fm) | $V_{so}$<br>(MeV) | $a_{so}$<br>(fm) | $r_{so}$<br>(fm) |
|--------|--------------|---------------|-------------|--------------|---------------|---------------|-------------------|------------------|------------------|
| Set I  | 95.          | 1.21          | 0.71        | 6.70         | 1.47          | 0.70          | 9.                | 0.9              | 0.6              |
| Set II | 112.         | 1.05          | 0.85        | 8.50         | 1.66          | 0.52          | 9.                | 0.9              | 0.6              |

4.4  $^{40}\text{Ca}(d,\alpha)^{38}\text{K}$  reactions.

$^{40}\text{Ca}(d,\alpha)^{38}\text{K}$  angular distributions were obtained at 4.50, 4.75, 5.00, 5.25 and 5.50 MeV. Since thin targets were used, and no averaging was done, these distributions are not expected to agree well with theoretical predictions. The experimental angular distributions are presented in figures 4.6 to 4.10. No theoretical calculations have been attempted.

Figure 4.6

$^{40}\text{Ca}(d,\alpha)^{38}\text{K}$  angular distributions.

Figure 4.7

$^{40}\text{Ca}(d,\alpha)^{38}\text{K}^{0.13}$  angular distributions.

Figure 4.8

$^{40}\text{Ca}(d,\alpha)^{38}\text{K}^{0.45}$  angular distributions.

Figure 4.9

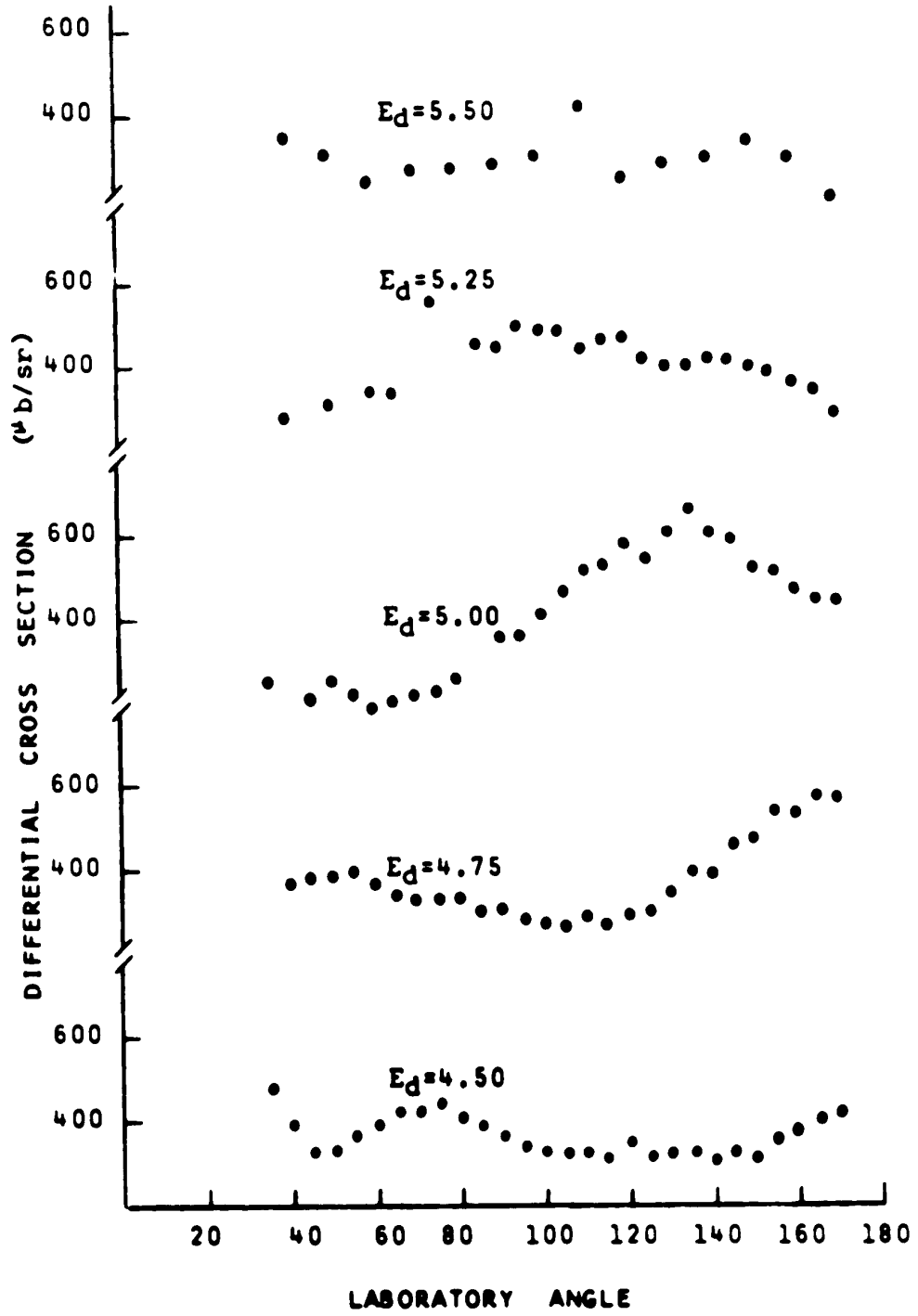
$^{40}\text{Ca}(d,\alpha)^{38}\text{K}^{1.7}$  angular distributions.

Figure 4.10

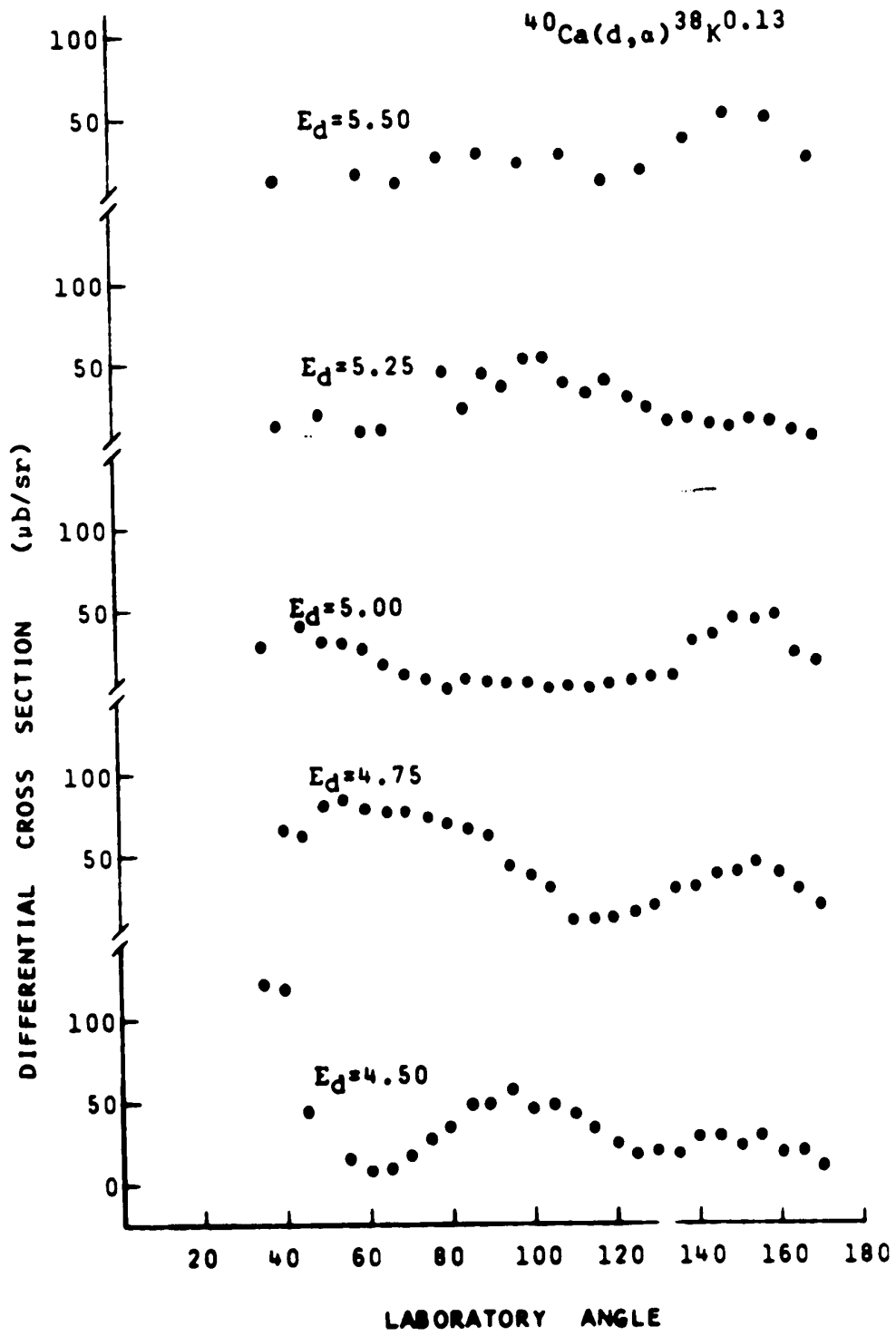
$^{40}\text{Ca}(d,\alpha)^{38}\text{K}^{2.41}$  angular distributions.

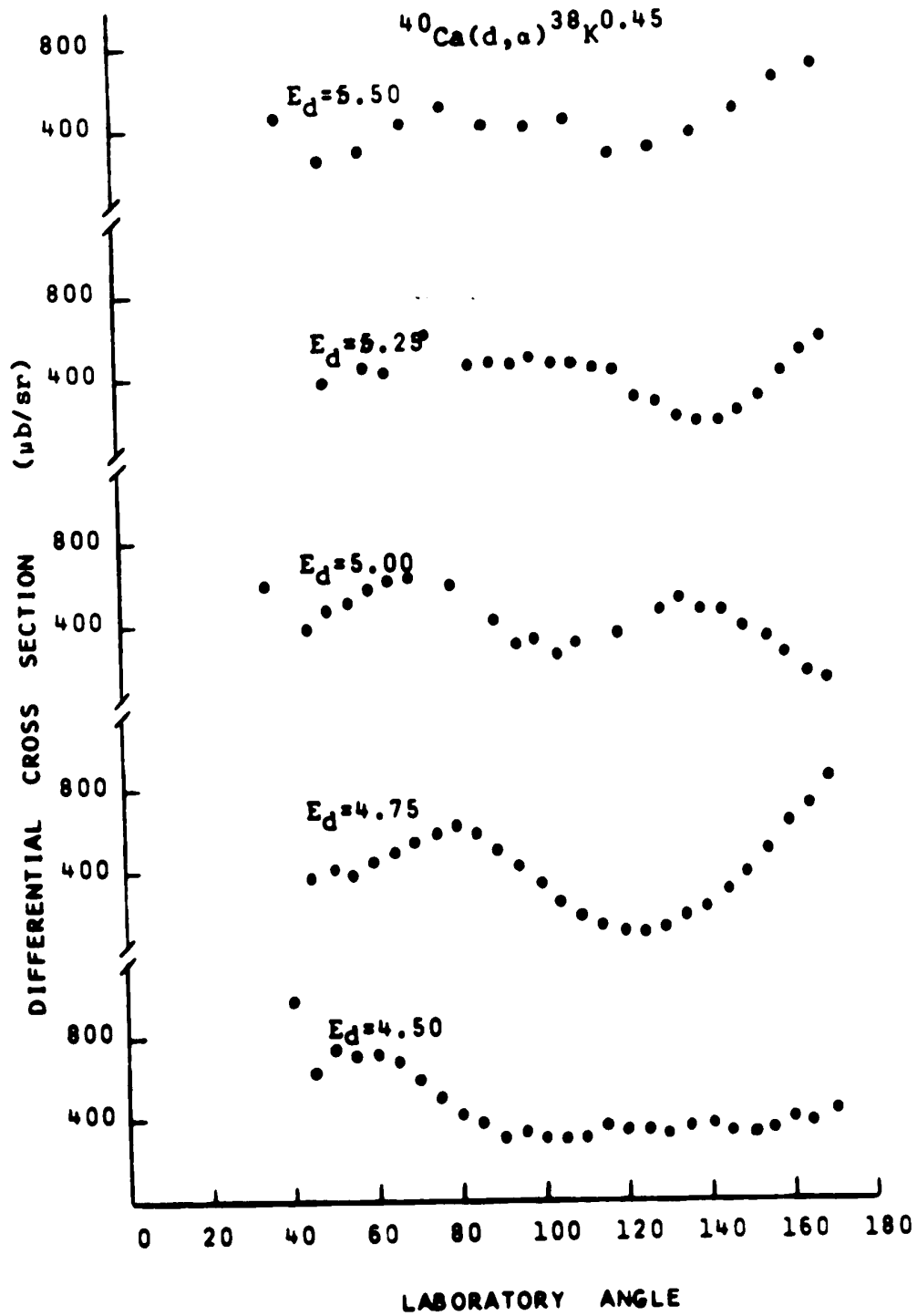
In all cases, the statistical error is less than the size of the data points.

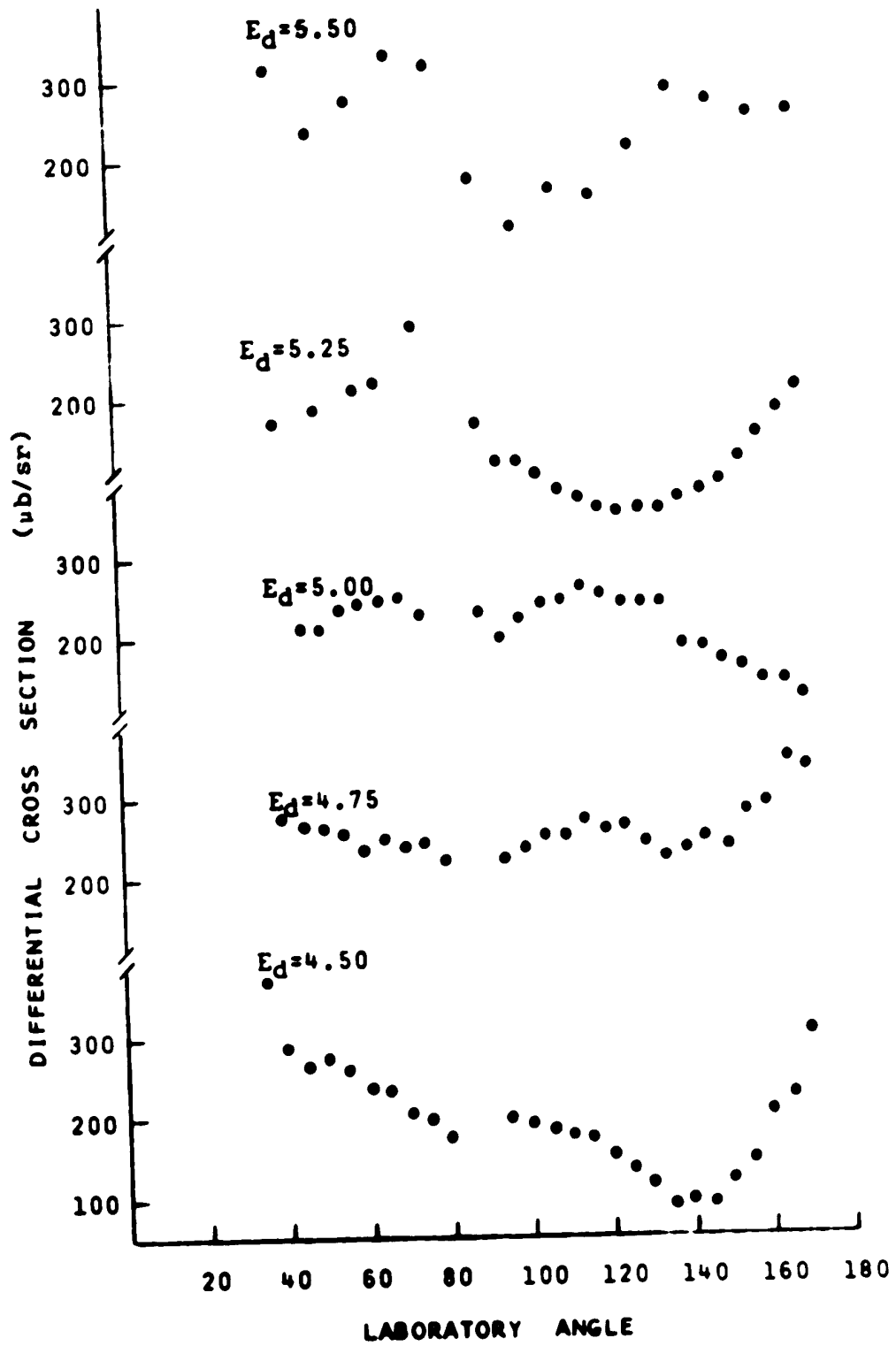
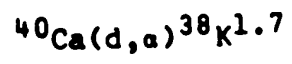
$^{40}\text{Ca}(d,\alpha)^{38}\text{Kgs}$



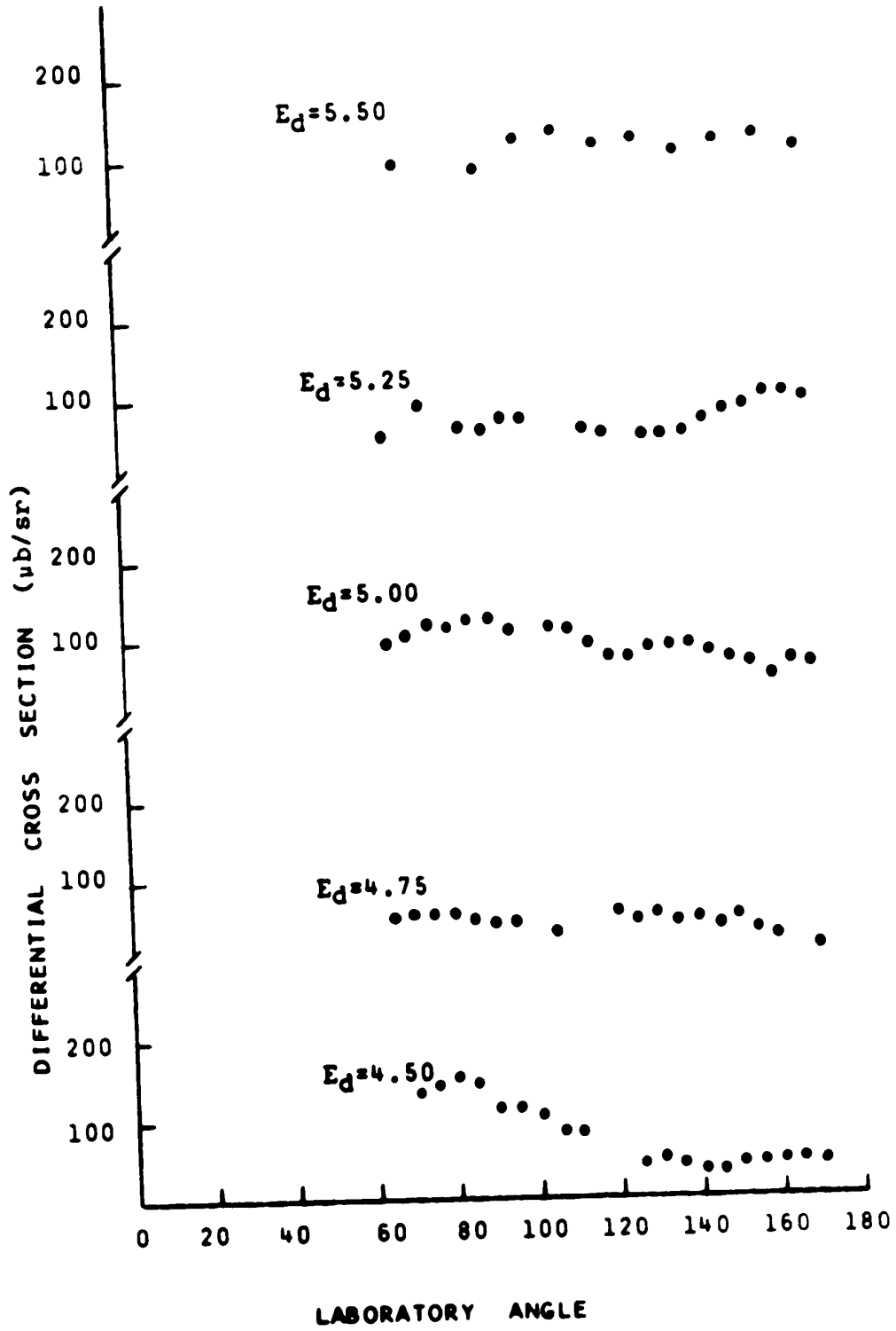








$^{40}\text{Ca}(d,\alpha)^{38}\text{K}^{2.41}$



#### 4.5 $^{40}\text{Ca}(d,p)^{41}\text{Ca}$ compound nuclear reactions.

Table 4.4 lists the energy levels of  $^{41}\text{Ca}$ , and is taken from En67. The levels are numbered according to the scheme of Be65.

In  $^{40}\text{Ca}(d,p)^{41}\text{Ca}$  reactions, many states in  $^{41}\text{Ca}$  are formed nearly exclusively by compound nuclear reactions. These states are characterized by low cross sections and relatively isotropic angular distributions. Cross sections for five such states (levels 7, 8, 9, 10 and 16) were measured between  $50^\circ$  and  $170^\circ$  in  $10^\circ$  increments, at energies from 4.50 MeV to 5.50 MeV in 2 keV steps. As mentioned in 3.2, the cross sections were automatically averaged over 50 keV energy increments, then averages over larger energy increments were done manually. The effect of the size of the energy averaging interval on the cross sections was investigated by averaging over 250 keV ( $\geq 10\Gamma$ ), 500 keV ( $\geq 20\Gamma$ ) and 1000 keV ( $\geq 40\Gamma$ ).

Figure 4.11 shows four angular distributions for state 9 obtained by averaging over different 250 keV intervals. Since the mean energy for each interval is different, absolute cross sections cannot be compared. However, we can compare the shapes of the distributions. It is frequently assumed that averaging cross sections over energy intervals of  $10\Gamma$  or  $20\Gamma$  is sufficient to remove fluctuations, making the results directly comparable to Hauser-Feshbach theory (e.g. St70, Bo69a). The distributions in figure 4.11 are averaged over  $\geq 10\Gamma$ ; therefore, if the above assumption is correct, we would expect very little change in shape for

Table 4.4

First 20 energy levels of  $^{41}\text{Ca}$  (En67) numbered according to scheme of Belote et al (Be65).

| <u>Level number</u> | <u>Excitation Energy (MeV)</u> |
|---------------------|--------------------------------|
| 0                   | 0                              |
| 1                   | 1.943                          |
| 2                   | 2.010                          |
| 3                   | 2.463                          |
| 4                   | 2.578                          |
| 5                   | 2.606                          |
| 6                   | 2.670                          |
| 7                   | 2.884                          |
| 8                   | 2.961                          |
| 9                   | 3.050                          |
| 9a                  | 3.122                          |
| 10                  | 3.200                          |
| 11                  | 3.369                          |
| 12                  | 3.400                          |
| 13                  | 3.495                          |
| 14                  | 3.527                          |
| 15                  | 3.614                          |
| 16                  | 3.676                          |
| 17                  | 3.730                          |
| 18                  | 3.831                          |
| 19                  | 3.845                          |
| 20                  | 3.915                          |

Figure 4.11

$^{40}\text{Ca}(d,p)^{41}\text{Ca}^{3.05}$  angular distribution  
(state 9). Averaged data, averaging interval = 250 keV.

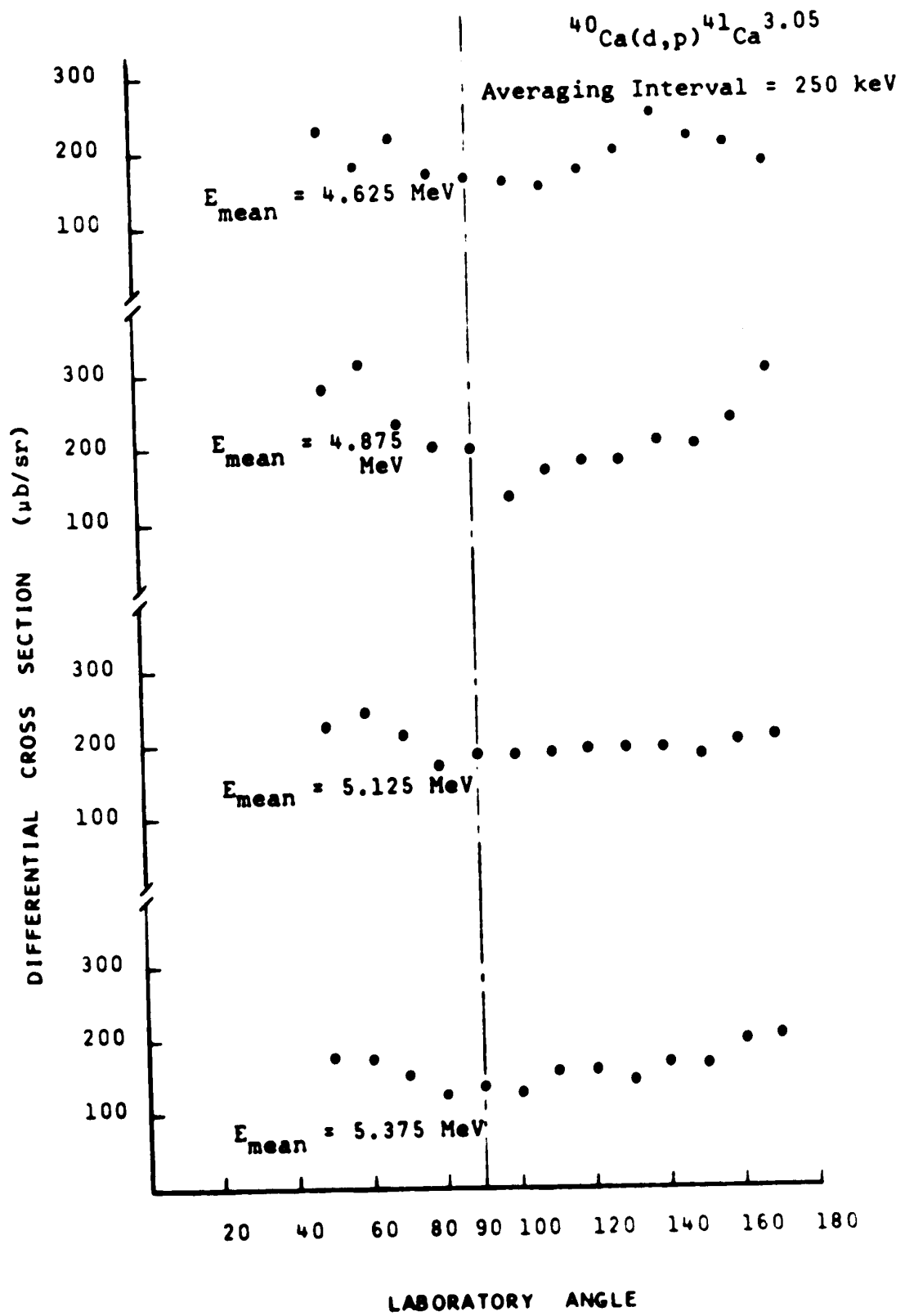
Figure 4.12

As in figure 4.11, but with averaging  
interval = 500 keV.

In both cases, the statistical error is less  
than the size of the data points.

Figure 4.13

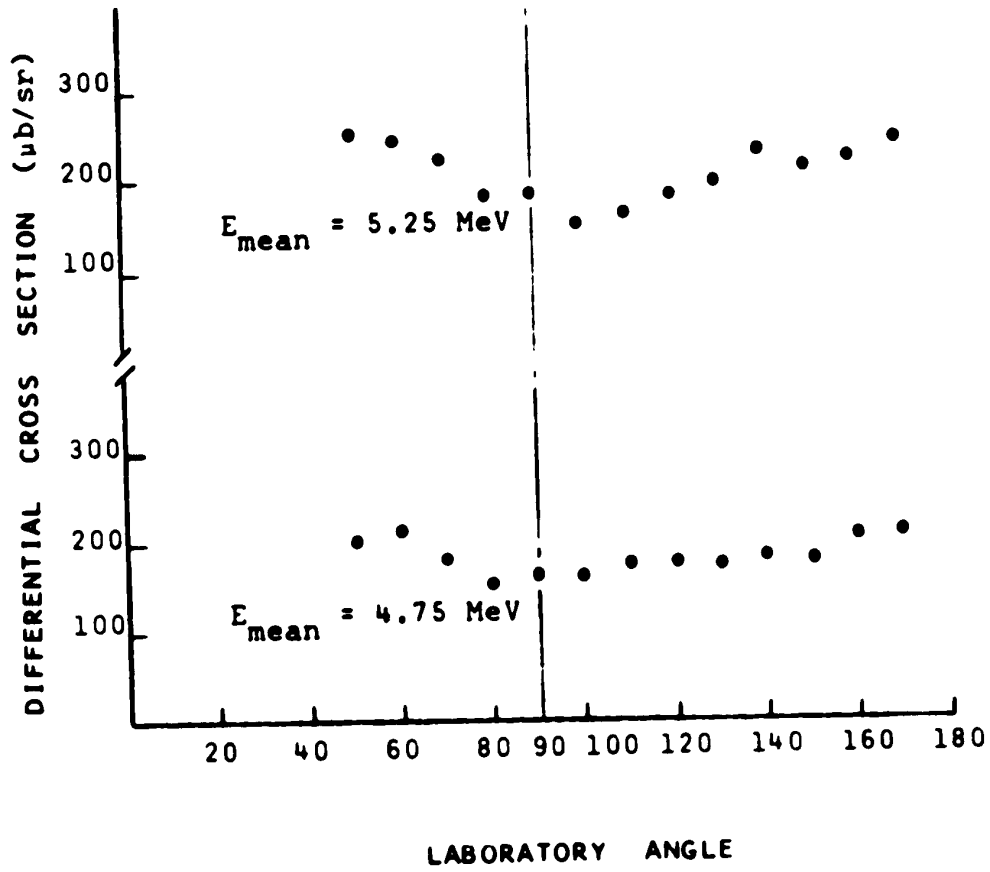
As in figure 4.11, but with averaging interval =  
1000 keV. The distribution is plotted twice; the upper  
curve with a scale comparable to that in figures 4.11 and  
4.12. Hauser-Feshbach predictions for several spins are  
shown. If no error bars are shown, the statistical  
error is less than the size of the data point.





$^{40}\text{Ca}(d,p)^{41}\text{Ca}^{3.05}$

Averaging Interval = 500 keV



$^{40}\text{Ca}(d,p)^{41}\text{Ca}^{3.05}$

Averaging Interval = 1 MeV

$E_{\text{mean}} = 5.00 \text{ MeV}$

— Hauser-Feshbach  
calculations

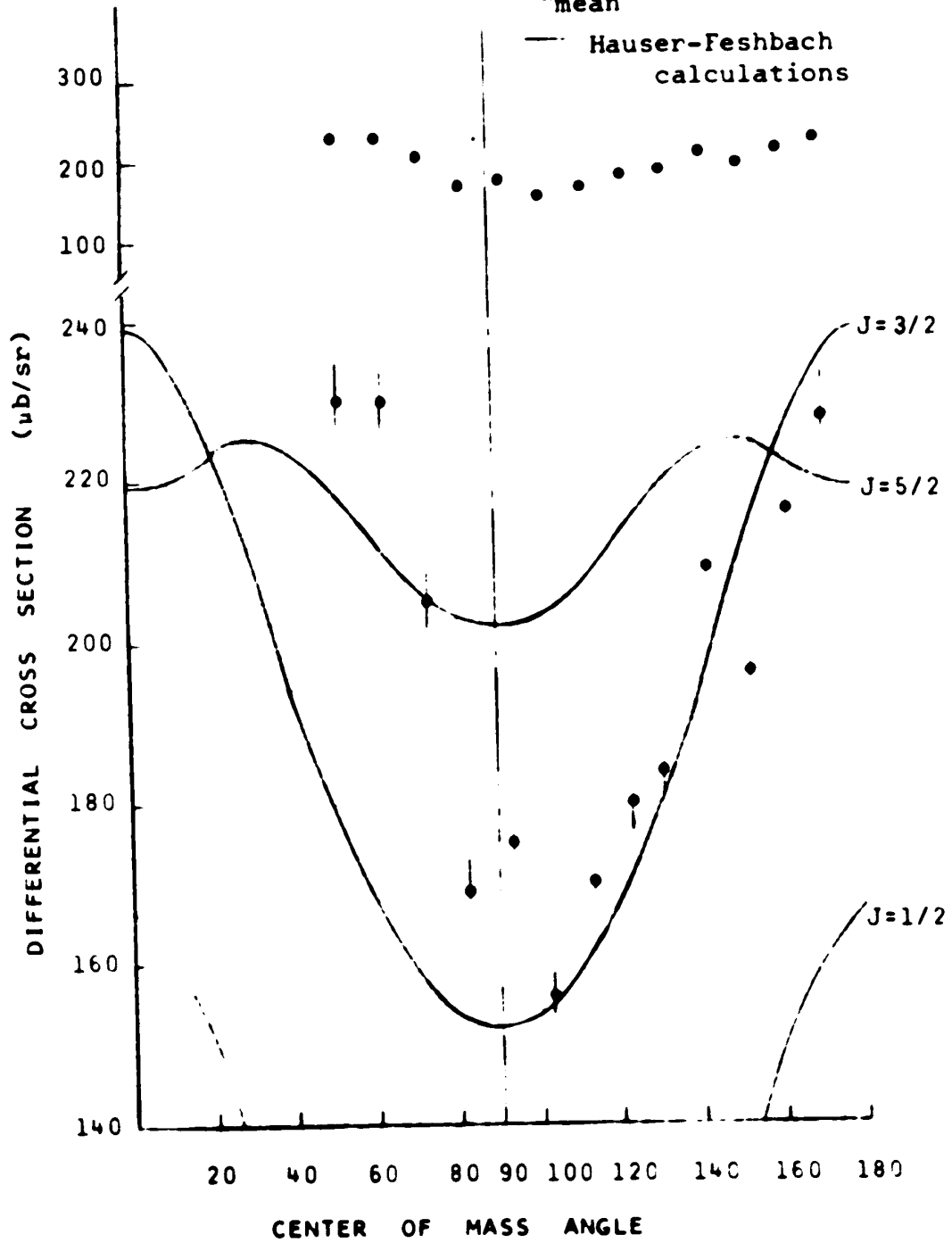


Figure 4.14

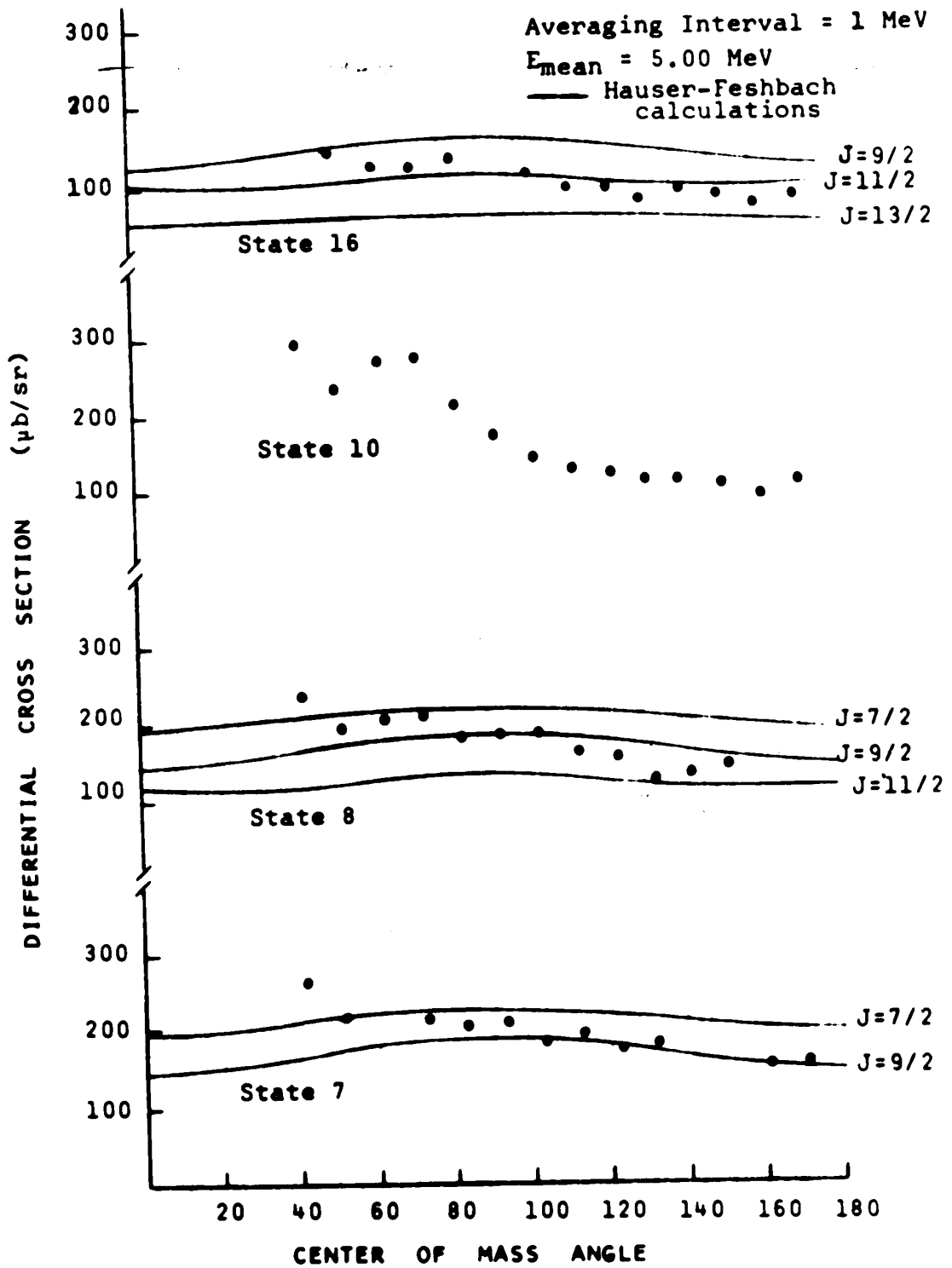
$^{40}\text{Ca}(d,p)^{41}\text{Ca}^*$  angular distributions for state 7 ( $^{41}\text{Ca}^{2.88}$ ), state 8 ( $^{41}\text{Ca}^{2.96}$ ), state 10 ( $^{41}\text{Ca}^{3.20}$ ) and state 16 ( $^{41}\text{Ca}^{3.68}$ ). Averaging interval = 1 MeV, mean bombarding energy = 5.00 MeV. Hauser-Feshbach calculations are given for states 7, 8 and 16.

$^{40}\text{Ca}(d,p)^{41}\text{Ca}^*$

Averaging Interval = 1 MeV

$E_{\text{mean}} = 5.00 \text{ MeV}$

— Hauser-Feshbach calculations



a different mean energy. This is obviously not the case. This suggests that the averaging interval may be too small. We would also expect symmetry of the angular distribution about  $90^\circ$  if the state is populated entirely by the compound nuclear mechanism. The observed asymmetry could arise from the energy averaging interval being too small, or from small contributions from the direct reaction mechanism, or both.

Figure 4.12 shows the results for an averaging interval of 500 keV ( $\approx 20r$ ). The shape still changes with energy and there is asymmetry about  $90^\circ$ .

In figure 4.13 the data have been averaged over the entire 1 MeV range of the data. The cross sections are much more symmetric about  $90^\circ$ . Since the averaging interval is now  $\approx 40r$ , it is suspected that fluctuations must have been averaged out, and that the remaining asymmetry is due to a small direct reaction contribution to the cross sections. A similar suggestion has been made in Wi66, when asymmetries were found in a state formed by the compound nuclear mechanism in the  $^{37}\text{Cl}(p, \alpha)^{34}\text{S}$  reaction, even after averaging over  $50r$ .

The other compound nuclear states considered (i.e. 7, 8, 10 and 16) behaved in a similar manner to state 9: the 250 keV and 500 keV averaging intervals seemed to be inadequate. The angular distributions of these states for a 1000 keV averaging interval are presented in figure 4.14.

Hauser-Feshbach calculations were made for every state considered in  $^{41}\text{Ca}$ , whether the state was formed primarily by the direct or compound nuclear mechanism.

Recall that in equation 2.8, the Hauser-Feshbach prediction for the differential cross section as a function of angle, there is a sum in the denominator of the transmission coefficients to all possible decay states. In this study, decays were possible leaving  $^{41}\text{Ca}$  excited at up to nearly 12 MeV. We only have information on the levels of  $^{41}\text{Ca}$  up to 6.8 MeV, and only a few spins and parities are known. In such cases, the sum over transmission coefficients to discrete states can be replaced by an integration, but for this we need to know the density of states as a function of their spin and excitation energy. The usual method of determining the density of states is as follows:

(1) the density  $\rho_J(E^*)$  of states of spin  $J$  of a nucleus is assumed to be factorable into a term dependent only on the excitation energy  $E^*$ , and another term dependent only on the spin  $J$ . The usual form for this is

$$\rho_J(E^*) = \rho(E^*) (2J+1) \exp \frac{-J(J+1)}{2\sigma^2}$$

where  $\sigma$  is a parameter called the spin cut-off parameter.  $\sigma$  was determined by fitting the above distribution to the distribution of levels of known spin in  $^{41}\text{Ca}$  (fig. 4.15)

(2) as mentioned in 5.1,  $\rho(E^*)$  is determined for a particular nucleus from a plot of  $\log N(E)$  vs  $\sqrt{E}$ , where  $N(E)$  is the number of states below an excitation energy  $E$ . Figure 4.16 is such a level density plot for  $^{41}\text{Ca}$ . The lone point at 8.65 MeV is obtained from S-wave neutron resonance measurements on  $^{40}\text{Ca}$ , including the effects of our spin

Figure 4.15

Spin distribution of states with known spin  
in  $^{41}\text{Ca}$ . The theoretical curve is calculated from

$$\rho_J \propto (2J+1)\exp\left(-\frac{J(J+1)}{2\sigma^2}\right)$$

with  $\sigma = 2.72$

Number of states with Spin J  
in  $^{41}\text{Ca}$

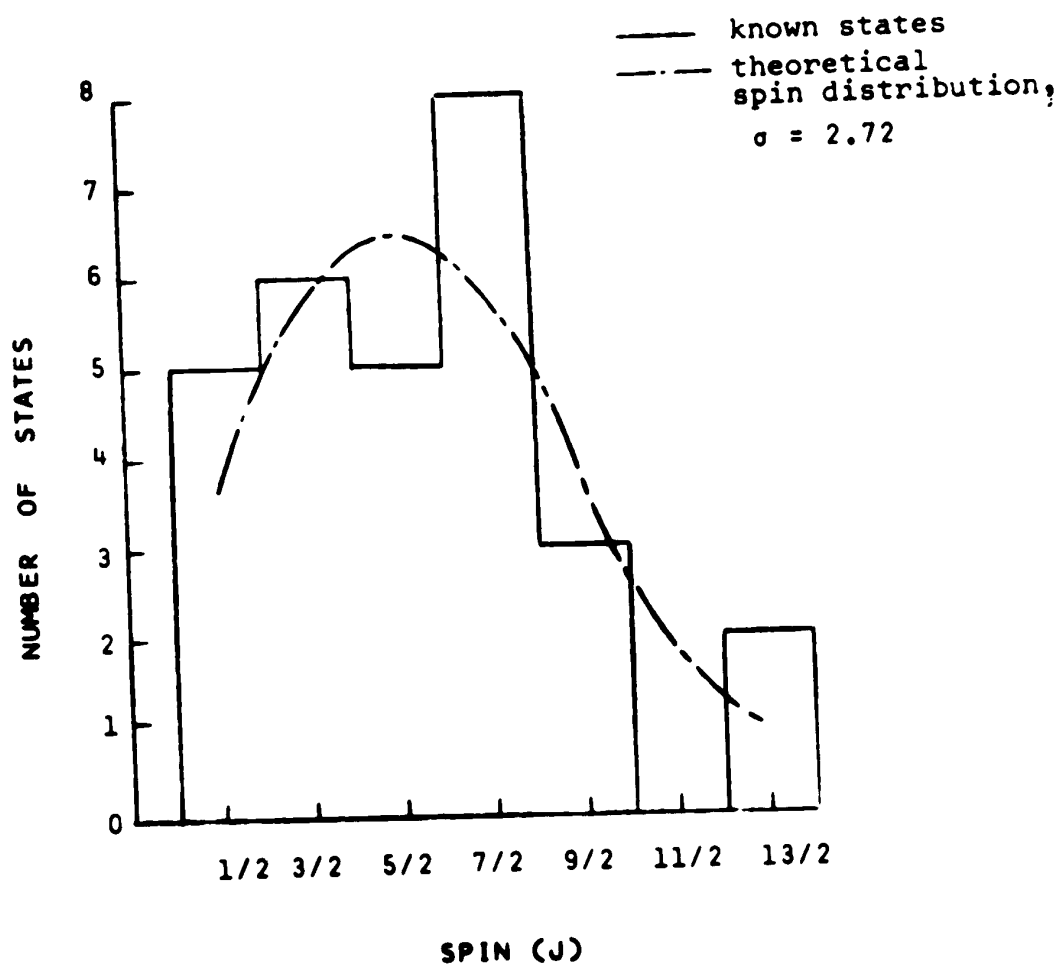
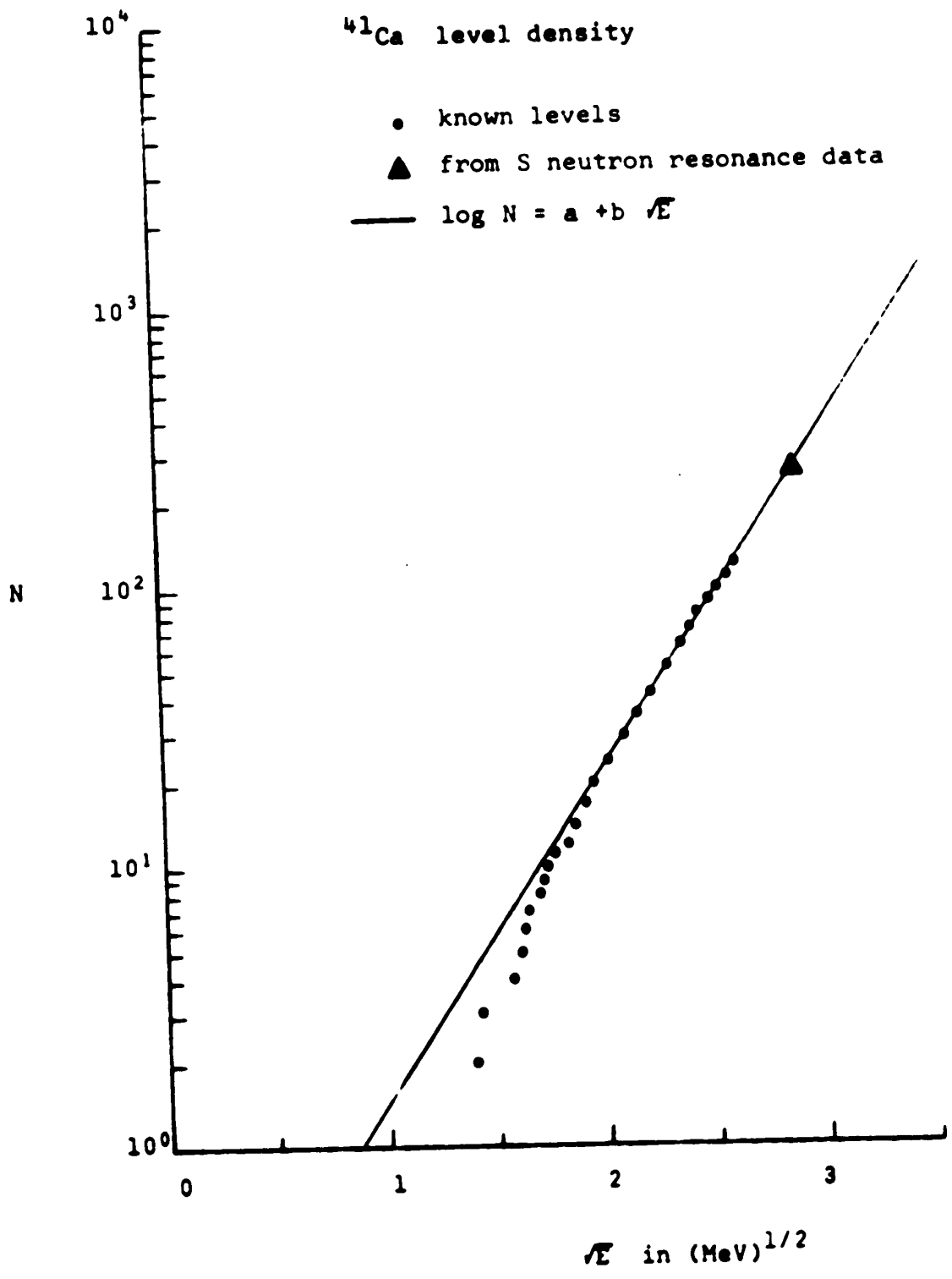




Figure 4.16

$^{41}\text{Ca}$  level density. The curve and the point were computed by G. Roy (Ro69) from the data of Bo62.



distribution.

Hauser-Feshbach calculations for the  $^{40}\text{Ca}(d,p)^{41}\text{Ca}$  reaction have been done previously at this laboratory by Roy and Davison (Ro69), using the program HAUSER. They compared the results of these calculations to the experimental measurements of Belote et al (Be65) at  $E_d = 7.0$  MeV. Many of the observed non-stripping states were adequately explained by the statistical model, and spin assignments were made. The level density of  $^{41}\text{Ca}$  was fixed very accurately by requiring the statistical model calculations to give the proper absolute magnitude for many non-stripping states.

In this study, similar calculations were done for the 1 MeV averaged  $^{40}\text{Ca}(d,p)^{41}\text{Ca}$  data. Several points concerning the calculations should be made:

- (1) The program HAUSER was used.
- (2) The calculations were insensitive to the deuteron optical model parameters used. Two sets of deuteron parameters were used: those obtained in this study from the 1 MeV averaged data, and those from Schwandt and Haeberli (Sc69). Both sets gave quite similar results.
- (3) The absorptive potential for the deuteron used in the Hauser-Feshbach calculation includes the effects of deuterons absorbed from the beam by direct reactions as well as those absorbed by compound nuclear reactions. This introduces an error into the predicted cross sections, since we are only considering compound nuclear

reactions in the calculation. The usual correction is calculated in the following way:

$$\sigma_{\text{CN}} = \left[ \frac{\sigma_{\text{tot}} - \sigma_{\text{D}}}{\sigma_{\text{tot}}} \right] \sigma_{\text{CN}}^1$$

Here  $\sigma_{\text{CN}}^1$  is the cross section given by the compound nucleus program,  $\sigma_{\text{CN}}$  is the corrected value to be compared with experiment,  $\sigma_{\text{tot}}$  is the total reaction cross section, and  $\sigma_{\text{D}}$  is the total direct interaction cross section.

In this investigation,  $\sigma_{\text{tot}}$  was calculated by the program SNOOPY, and  $\sigma_{\text{D}}$  was estimated by DWUCK calculations using the experimental spectroscopic factor (see section 4). The (d,n) direct cross section was calculated from the data of Leighton et al (Le68). This gave a correction factor of .60.

(4) The level density used for  $^{41}\text{Ca}$  was that obtained by Roy and Davison in Ro69. Other level densities were obtained from plots of  $N(E)$  vs.  $\sqrt{E}$ , as explained previously.

(5) Since energy averages of the experimental data were taken over considerable energy intervals, i.e. up to 1 MeV, HAUSER calculations were done over the same interval in 25 keV steps. The theoretical cross sections were then energy averaged before comparison with the energy averaged data.

(6) There has been no arbitrary normalization of the HAUSER predictions. Absolute cross sections are calculated, and are directly comparable to the data (after correcting for direct interactions).

The results of these calculations are partially given in figures 4.13 and 4.14, where they are compared with states in  $^{41}\text{Ca}$  that are thought to be formed primarily by the compound nuclear mechanism. As mentioned previously, despite averaging of the data over  $>40^\circ$ , and careful attention to background estimation, electronic dead time and target non-uniformity, the experimental angular distributions of these states are not symmetric about  $90^\circ$ . They are slightly peaked in the forward quadrant, suggesting a small admixture of the direct reaction mechanism.

In four of the five states considered (7, 8, 9 and 16) the angular distribution is fairly symmetric, and H-F calculations were done in these cases. Peak 10, however, is strongly peaked, and no calculation was attempted.

State 7 has  $J^\pi = (7/2^+)$  (Jo69). HAUSER predictions for spins  $7/2$  and  $9/2$  both give reasonable fits to the data.

State 8, measured as  $J^\pi = (7/2^-)$  (Jo69), is fairly asymmetric about  $90^\circ$ . HAUSER calculations for spins  $7/2$ ,  $9/2$  and  $11/2$  give reasonable values for the absolute cross sections, if not the shape of the angular distribution.

Johnson (Jo69) found state 9 to have spin  $3/2$  or  $5/2$ . The 1 MeV averaged data for this state give an angular distribution that is fairly symmetric about  $90^\circ$ . HAUSER predictions for spin  $3/2$  and spin  $5/2$  both give acceptable

fits to the data.

The spin of state 16 has not been measured. Spins of  $9/2$ ,  $11/2$  and  $13/2$  give fair HAUSER predictions for this state.

#### 4.6 $^{40}\text{Ca}(d,p)^{41}\text{Ca}$ direct reactions.

Cross sections for states in  $^{41}\text{Ca}$  formed predominantly via the direct reaction mechanism were calculated theoretically using the DWBA code DWUCK<sup>†</sup>. All calculations used a finite range parameter  $\beta = 0.60 \text{ fm}^{-1}$  and nonlocality ranges of 0.50 fm for the deuteron, and 0.85 fm for the neutron and the proton. The optical model parameters used in these calculations are given in table 4.5. The deuteron parameters are those obtained in this investigation from the elastic scattering data and the proton parameters are those of Greenlees and Pyle (Gr66). For the neutron, the depth of the central well is adjusted by the program so that the binding energy of the well is equal to the experimental separation energy, the spin-orbit radius and diffuseness are the same as for the central well. Thus there are three undetermined parameters: the radius  $r_{so}$ , the diffuseness  $a_{so}$  and the depth  $V_{so}$  of the spin-orbit potential. These were taken from the work of Ferey and Buck (Pe62).

Table 4.5

Optical model parameters used in DWBA calculations.

Units MeV or fm.

| Particle | V                        | r    | a    | W    | $R_i$ | $a_i$ | $V_{so}$ | $a_{so}$ | $r_{so}$ |
|----------|--------------------------|------|------|------|-------|-------|----------|----------|----------|
| deuteron | 95                       | 1.21 | 0.71 | 6.70 | 1.47  | 0.70  | 9.       | 0.9      | 0.6      |
| proton   | 55<br>-0.3E <sub>p</sub> | 1.20 | .70  | 6.0  | 1.25  | 0.70  | 6.0      | 1.10     | 0.70     |
| neutron  | --                       | 1.27 | 0.66 | --   | --    | --    | 7.2      | 1.27     | 0.66     |

<sup>†</sup>Obtained from P.D. Kunz, University of Colorado, Boulder, Colo.

Sample calculations were also done using the deuteron parameters of Sc69. The results were not significantly different, and are not presented here.

The states at 0.0, 1.943, 2.010 and 2.463 MeV excitation (states 0, 1 and 3) were selected for detailed consideration. These states have relatively high (d,p) cross sections and are well separated from adjacent peaks.

In the shell model, we picture  $^{40}\text{Ca}$  as a very inert nucleus, with neutrons and protons filling all shell model levels up to the  $1\text{d}_{3/2}$  level inclusive. Ideally, we could think of  $^{41}\text{Ca}$  as a single neutron orbiting in a potential created by the inert  $^{40}\text{Ca}$  core. The ground state of  $^{41}\text{Ca}$  would then be a neutron in the  $1\text{f}_{7/2}$  shell model orbit plus the inert core. As explained in section 2.2, DWBA calculations are done assuming this simplified picture to be true. The ratio of experimental cross sections to DWBA predictions gives the spectroscopic factor, which is a measure of the validity of the above model, i.e. a measure of the single particle character of the state. Experimentally, we know that it is very difficult to excite protons or neutrons in the  $^{40}\text{Ca}$  nucleus (it is "doubly magic"), so it should be a very inert core in  $^{41}\text{Ca}$ . Thus, we expect that at least the ground state, and possibly some excited states, should correspond very well to the model of a single particle orbiting an inert core. Because of these properties,  $^{41}\text{Ca}$  has been rather extensively investigated. In Le68, the  $^{40}\text{Ca}(\text{d},\text{p})^{41}\text{Ca}$  reaction was done at 5.0 MeV, and angular distributions for states 0, 1 and 3 were



obtained. These distributions are given in figs. 4.17, 4.18 and 4.19. DWBA calculations were performed, but fits were poor in the backward quadrant, particularly for the ground state. Part of the purpose of the present investigation was to see if the poor fits at back angles (where the compound nucleus mechanism is most important in a stripping reaction) could be improved by obtaining energy averaged cross sections, thereby eliminating the effects of compound nuclear fluctuations. DWBA calculations were done from 4.5 to 5.5 MeV in 25 keV steps, and the results were energy averaged. The angular distributions obtained in this way were slightly different in shape and magnitude from those calculated at the mean energy.

Figures 4.17, 4.18 and 4.19 give the unaveraged data of Leighton (Le68), and the 1 MeV averaged data and DWUCK calculations from the present investigation. Compound nuclear contributions were calculated using HAUSER, and subtracted from both sets of experimental data.

For the ground state (state 0), the 1 MeV average greatly affects the experimental cross sections at angles greater than  $90^\circ$ , and improves the agreement between theory and experiment. The resulting spectroscopic factor is 0.83.

The averaged distributions for states 1 and 3 have different shapes from those of Leighton at back angles, but there is no improvement in the fit of the DWUCK calculations to the data. There is a difference in the absolute cross sections also. The spectroscopic factors obtained for states 1 and 3 in the present investigation are 0.37 and 0.13.

Figure 4.17

- $^{40}\text{Ca}(d,p)^{41}\text{Ca}^{0.0}$  angular distributions:
- 1 MeV averaged data from this study,  $E_{\text{mean}} = 5.00$  MeV
  - Data of Leighton,  $E_d = 5.00$  MeV
  - DWBA fit to data,  $S = 0.83$

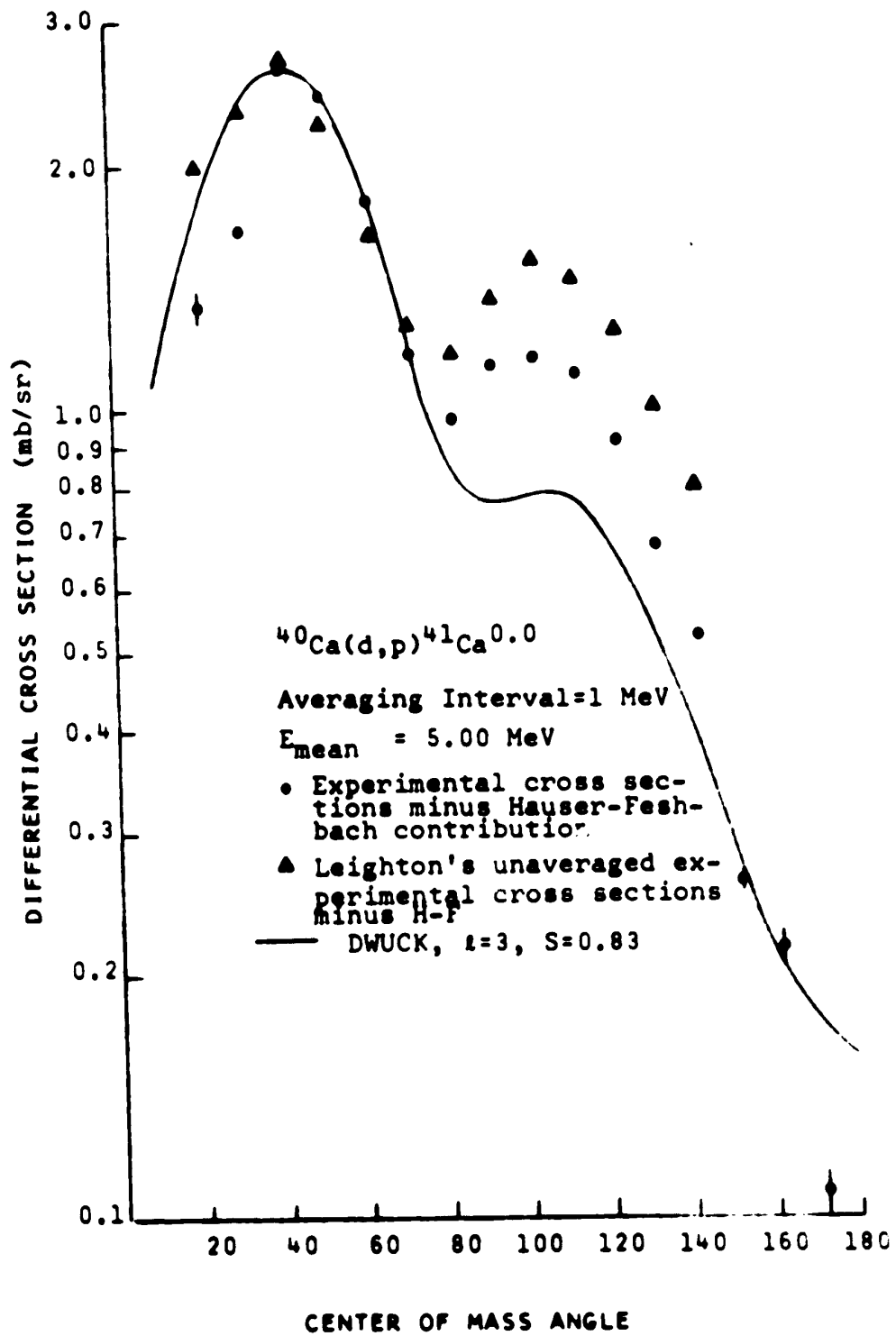


Figure 4.18

$^{40}\text{Ca}(d,p)^{41}\text{Ca}^{1.95}$  angular distributions:

-- 1 MeV averaged data from this study,  $E_{\text{mean}} = 5.00$  MeV

-- Data of Leighton,  $E_d = 5.00$  MeV

-- DWBA fit to data,  $S = 0.37$

$^{40}\text{Ca}(d,p)^{41}\text{Ca}^{1.95}$

1 MeV averaging interval

$E_{\text{mean}} = 5.00 \text{ MeV}$

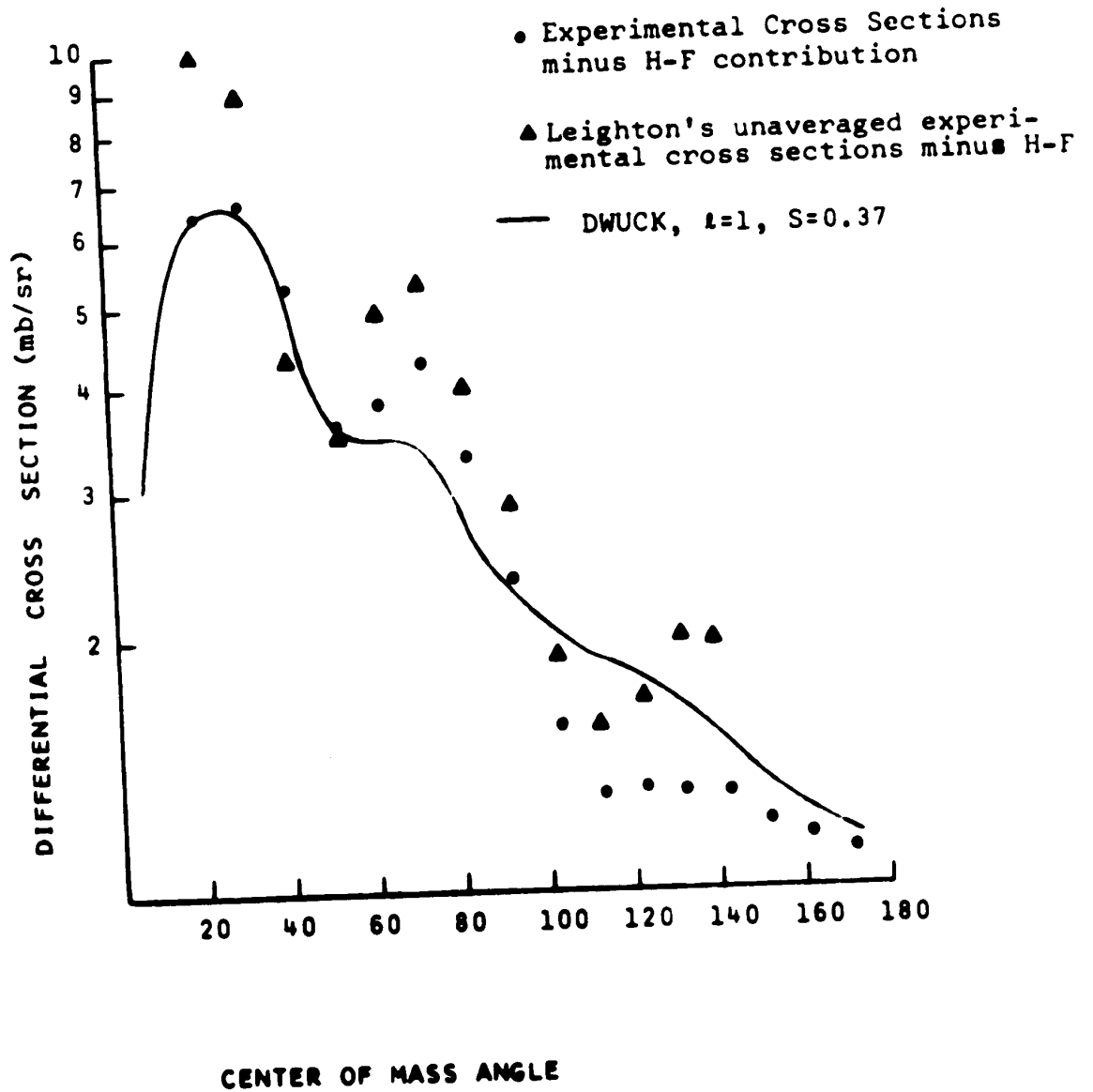


Figure 4.19

$^{40}\text{Ca}(d,p)^{41}\text{Ca}^{2.46}$  angular distributions:

- 1 MeV averaged data from this study,  $E_{\text{mean}} = 5.00$  MeV
- Data of Leighton,  $E_d = 5.00$  MeV
- DWBA fit to data,  $S = 0.13$

$^{40}\text{Ca}(d,p)^{41}\text{Ca}^{2.46}$

Averaging Interval = 1 MeV

$E_{\text{mean}} = 5.00 \text{ MeV}$

• Experimental Cross Sections  
minus Hauser-Feshbach contribution

▲ Leighton's unaveraged experimental cross sections minus H-F

— DWUCK,  $l=1$ ,  $S=0.13$

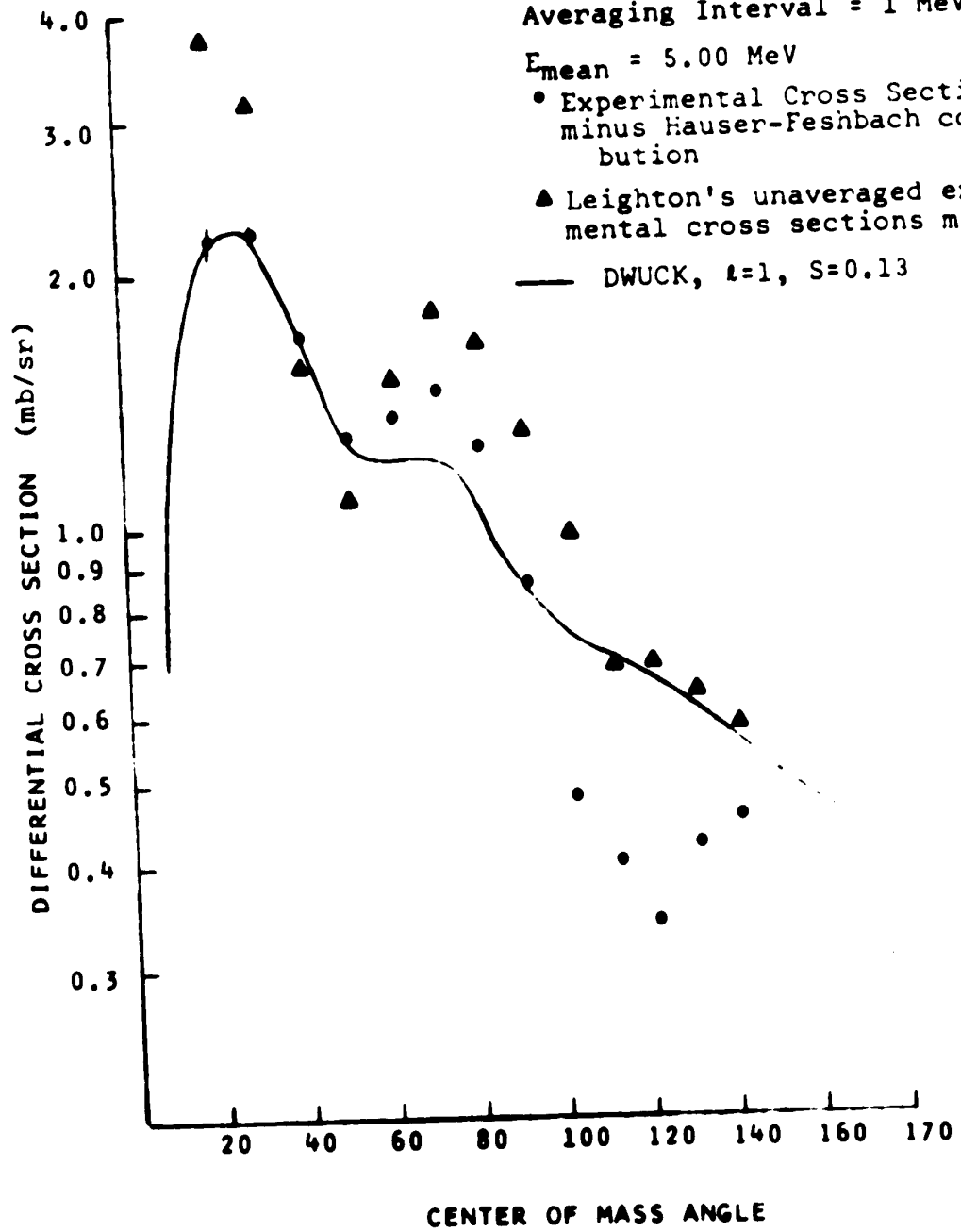
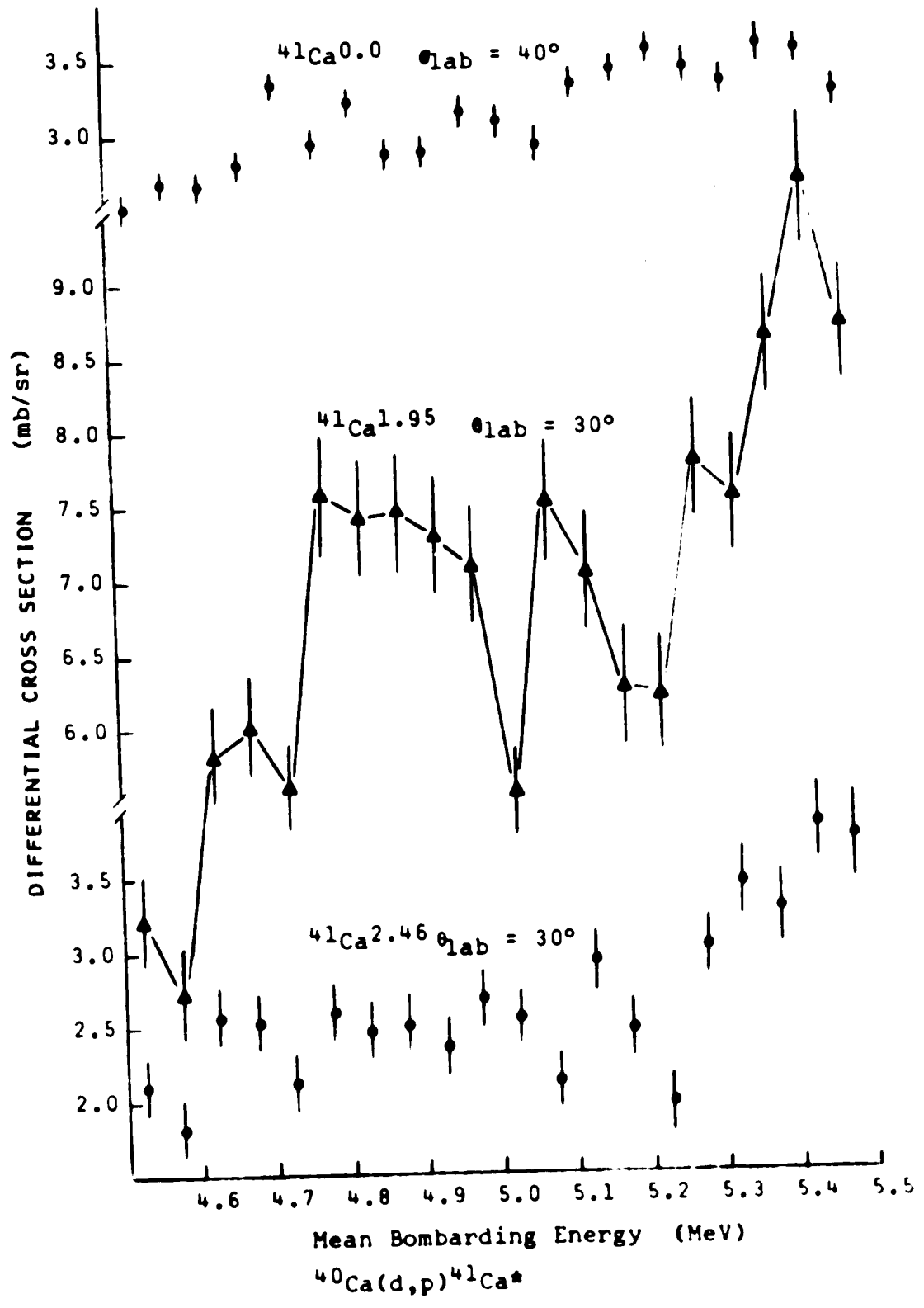


Figure 4.20

Yield curve of  $^{40}\text{Ca}(d,p)$  leaving  $^{41}\text{Ca}$  in ground state, first and third excited states. Cross sections are averaged over 50 keV. Measurements were made at an angle near the stripping peak.





The values for the spectroscopic factors are different from those obtained by previous investigators. Table 4.6 summarizes the values obtained from this study, those of Leighton et al (Le68) obtained at 5.00 MeV, those of Lee, Schiffer et al (Le64) which are averaged over the range 7 - 12 MeV, and those of Seth et al (Se70) obtained at 12.0 MeV.

Table 4.6

| Spectroscopic factors for states in $^{41}\text{Ca}$ |            |             |             |
|--|------------|-------------|-------------|
| <u>State</u>   | <u>0.0</u> | <u>1.95</u> | <u>2.46</u> |
| <u>Source</u>  |            |             |             |
| This study   | 0.83       | 0.37        | 0.13        |
| Leighton et al                                       | 0.68       | 0.50        | 0.19        |
| Lee et al  | 0.86       | 0.72        | 0.32        |
| Seth et al   | 0.76       | 0.67        | 0.21        |

The work of Lee, Schiffer et al and Seth et al was done at high enough energies that the compound nuclear contribution to cross sections is negligible. We therefore believe the spectroscopic factors deduced in those studies to be better than those obtained at lower energies.

Referring to table 4.6, we note that the spectroscopic factors obtained in this study for the 1.95 MeV and 2.46 MeV states in  $^{41}\text{Ca}$  are in substantial disagreement with the values obtained at higher energy. We further note the disagreement between the spectroscopic factors obtained in the present study (averaged data, mean bombarding energy = 5.00 MeV) and those obtained by Leighton (data taken at

one energy: 5.00 MeV).

Upon inspection of figure 4.20, at least part of the reason for the discrepancies becomes apparent. Figure 4.20 is a yield curve for states 0, 1 and 3 taken at angles near their respective stripping peaks. Since the compound nuclear contribution to the cross sections is relatively small ( $<300 \mu\text{b/sr}$ ) we expect the direct reaction mechanism to predominate. Thus, a smooth yield curve is expected. The yield for the ground state is indeed fairly smooth and the spectroscopic factor obtained is close to the high energy value. However, minor fluctuations are present. The other yield curves have much more structure, especially the one for the 1.95 MeV state. It was surprising to find such large fluctuations in the cross section of a direct state at the stripping peak. It implies that spectroscopic factors deduced by measuring cross sections at one energy in this range must be viewed with some suspicion. In fact, if we accept the spectroscopic factors measured at higher energy as being correct, our method of measuring cross sections in small steps over a range of 1 MeV and averaging them is not sufficient to remove the effects of the structure of the yield curve and give good spectroscopic factors.

#### 4.7 Summary and Conclusions.

- (1) The average width of levels in  $^{42}\text{Sc}$  at  $\sim 15$  MeV excitation has been found to be  $\Gamma \leq 23$  keV.
- (2) Data for  $^{40}\text{Ca}(d,p)^{41}\text{Ca}$  reactions were obtained between 4.50 MeV and 5.50 MeV in 2 keV steps. Energy averaged cross sections were extracted from these data. Averaging intervals of  $\geq 10\Gamma$  and  $\geq 20\Gamma$  were found to be inadequate to average out compound nuclear fluctuations. An averaging interval of  $\geq 40\Gamma$  still gave angular distributions for states 7, 8, 9, 10 and 16 that were not symmetric about  $90^\circ$ . (These states are expected to be formed nearly entirely by the compound nuclear mechanism.) The asymmetry was attributed to a small but significant contribution from the direct reaction mechanism, giving a peaking at forward angles.
- (3) Comparison of the 1 MeV averaged data (mean energy - 5.00) for states 0, 1 and 3 with unaveraged data obtained by Leighton at 5.00 MeV showed changes in relative and absolute cross sections. This was not expected at forward angles where the direct mechanism predominates, and suggests that cross sections should be energy averaged before comparison with DWBA calculations. Comparison of spectroscopic factors obtained from this data with reliable spectroscopic factors obtained at higher energies showed that an averaging interval of 1 MeV is sufficient to remove the effect of these fluctuations on the spectroscopic factor obtained for the ground state of  $^{41}\text{Ca}$ . The spectroscopic factors of the first and third excited states obtained from

the 1 MeV averaged data do not agree with the high energy spectroscopic factors. This suggests that an averaging interval of 1 MeV is not sufficient in these cases.

In view of the unexpected large fluctuations in the cross section of the first excited state at its stripping peak, it is suggested that in the future, before accepting a spectroscopic factor measurement, yield curves should be taken on the stripping peak to establish that the yield varies smoothly in the energy range of interest.

(4) The agreement between experiment and DWBA at back angles for the ground state of  $^{41}\text{Ca}$  was improved if 1 MeV averaged data were used rather than unaveraged data.

(5) The above procedure did not improve the fit for the 1.943 and 2.463 states of  $^{41}\text{Ca}$ .

## REFERENCES

- Be65 T. A. Belote, A. Sperduto and W. W. Buechner,  
Phys Rev 139, B 80 (1965)
- Bi52 L. C. Biedenharn, J. M. Blatt and M. E. Rose,  
Rev Mod Phys 24, 249 (1952)
- Bi70 A. E. Bisson, K. A. Eberhard and R. H. Davis,  
Phys Rev C1, 539 (1970)
- Bo62 C. D. Bowman, E. G. Bilpuch and H. W. Newson,  
Ann Phys 17, 319 (1962)
- Bo69 J. J. W. Bogaards, Thesis, University of  
Alberta (1969)
- Bo69a A. Bottega, W. R. McMurray and W. J. Naude,  
Nucl Phys A136, 265 (1969)
- Bu64 P. J. A. Buttle and L. J. B. Goldfarb,  
Proc Phys Soc 83, 701 (1964)
- Da65 P. J. Dallimore and I. Hall, Phys Lett 18, 138 (1965)
- Da69 N. E. Davison, private communication (1969)
- En66 H. A. Enge, Introduction to Nuclear Physics  
(Addison - Wesley, 1966)
- En67 P. M. Endt and C. van der Leun, Nucl Phys  
A105, 1 (1967)
- Er63 T. Ericson, Annals of Physics 23, 390 (1963)
- Fe65 F. P. Feynman, R. B. Leighton and M. Sands,  
The Feynman Lectures, Vol III (Addison - Wesley, 1965)
- Gr66 G. W. Greenlees and G. J. Pyle, Phys Rev 149,  
836 (1966)
- Ha52 W. Hauser and H. Feshbach, Phys Rev 87, 366 (1952)
- Hj65 S. A. Hjorth, J. X. Saladin and G. R. Satchler,  
Phys Rev 138, B 1465 (1965)
- Jo69 G. Johnson, Thesis, Orsay Faculty of Sciences,  
University of Paris (1969)
- Le64 L. L. Lee, J. P. Schiffer, B. Zeidman, G. F. Satchler,  
R. M. Drisko and R. H. Bassel, Phys Rev 136, B 971 (1964)
- Le68 H. G. Leighton, G. Roy, D. P. Gurd and T. E. Grandy,  
Nucl Phys A109, 218 (1968)

- Mi65 S. Micheletti and P. Mukherjee, Nucl Phys 63,  
504 (1965)
- Pa64 G. Pappalardo, Phys Lett 13, 320 (1964)
- Pe62 F. G. Perey and B. Buck, Nucl Phys 32, 353 (1962)
- Pe64 F. G. Perey and D. S. Saxon, Phys Lett 10,  
107 (1964)
- Pi70 A. A. Pilt, D. M. Sheppard, W. C. Olsen, T. P. G.  
Carola and P. J. Twin, Nucl Phys A150, 439 (1970)
- Ro69 G. Roy and N. Davison, Bull Amer Phys Soc, 14,  
1231 (1969)
- Ro69a G. Roy and N. Ribbeck, Nucl Instr and Meth 71,  
234 (1969)
- Ro71 G. Roy and L. Holm, to be published
- Sc69 P. Schwandt and W. Haeberli, Nucl Phys A123,  
401 (1969)
- Se70 K. K. Seth, J. Picard and G. R. Satchler, Nucl  
Phys A140, 577 (1970)
- St70 U. Strohmusch, W. Bakowsky and H. Lacey, Nucl Phys  
A149, 605 (1970)
- Vo69 E. Vogt in Advances in Nuclear Physics 1, Baranger  
and Vogt Eds (Plenum Press, 1969)
- Wi66 W. Von Witsch, P. von Brentano, T. Mayer-Kuckuk  
and A. Richter, Nucl Phys 80, 394 (1966)